Dual-BONCAT Reveals Distinct Subpopulations of Anabolically Active Cells

Dylan Mankel[a], Yasheng Maierhaba[a*], Claire Momjian[a^],
Federica Calabrese[a], Solange Duhamel[b], Jeffrey Marlow[a#]

[a]Department of Biology, Boston University, Boston, MA, USA
[b]Department of Molecular and Cellular Biology, University of Arizona, Tucson, AZ, USA

Running Head: Dual-BONCAT

#Address correspondence to Jeffrey Marlow, jjmarlow@bu.edu
*Present address: Dana-Farber Cancer Institute, Boston, MA, USA
^Present address: Cedars-Sinai Health Sciences University, Los Angeles, CA, USA

Dylan Mankel and Maierhaba Yasheng contributed equally to this work; author order was determined on the basis of seniority.

Abstract

Bio-Orthogonal Non-Canonical Amino Acid Tagging (BONCAT) has emerged as a prominent molecular technique that enables microbial ecologists to visualize and identify metabolically active cells in cultures and complex microbial communities. To date, researchers have used just one non-canonical amino acid (ncAA) in a given experiment; here, we validate a novel approach using two different ncAAs in a single experiment. This advancement facilitates the detection of differentially active subpopulations within the same experimental context, thereby reducing the uncertainty and variability associated with parallel treatments, and providing precise spatial information about organisms that are active under distinct conditions or at different times. We show that both ncAAs can be taken up by *E. coli* cultures and by constituents of the Little Sippewissett Salt Marsh microbiome, resulting in fluorescence signals that are significantly higher than background and ncAA-free control experiments, as well as differential labeling patterns reflective of distinct subpopulations. As a proof of concept, we implemented this "dual-BONCAT" approach in salt marsh sediments, adding one ncAA during daytime hours and the other at night. Subpopulations of cells that were anabolically active during the day and/or night were distinguishable by both fluorescence microscopy, and by fluorescence-activated cell sorting. Subsequent high-throughput 16S rRNA gene amplicon sequencing of active subpopulations revealed that *Methylobacterium*, potentially feeding on plant exudate carbon, was preferentially active during the day, while sulfur-cycling taxa dominated the night-active population. Dual-BONCAT offers an important advancement in multiplexing substrate-analog probing techniques, providing a more realistic understanding of metabolic activity under distinct environmental conditions.

Importance

Microbial communities are complex and dynamic, with different groups of microbes active under distinct conditions. Bio-Orthogonal Non-Canonical Amino Acid Tagging (BONCAT) uses synthetic amino acids to tag newly made proteins, allowing researchers to see and identify the active subset of a community. While BONCAT studies to date have used a single synthetic amino acid to evaluate cell activity in a single experimental context, here we introduce a new approach, "dual-BONCAT," using two synthetic amino acids to track differential responses to changing conditions. After validating the approach with *E. coli*, we deployed it in a salt marsh sediment community, finding that organisms potentially feeding on plant root sugars were more active during the day, and microbes likely metabolizing sulfur were more active at night. We believe dual-BONCAT will prove useful in many studies, as it illuminates microbial community responses to changing conditions, which has important implications for ecosystem dynamics.

Introduction

Understanding the metabolic activity of microbes in both controlled cultures and environmental communities is a major goal for microbiologists. Substrate analog probing techniques, which use analog molecular constituents to track assimilatory processes (1–3), have been adapted for use in environmental communities (4, 5). One such approach is Bio-Orthogonal Non-Canoncial Amino Acid Tagging (BONCAT), which relies on the cellular uptake of the non-canonical amino acids (ncAAs) *L*- azidohomoalanine (AHA) and *L*-homopropargylglycine (HPG), which can be incorporated into newly synthesized proteins in place of *L*-methionine without substantially affecting cell function (5, 6). AHA and HPG possess chemically modifiable azide and alkyne groups, respectively, to which fluorescently tagged molecules can be bound through "click chemistry" reactions (7, 8). Recent validation of β-ethynylserine as a threonine

47 analog amenable to click reactions in a range of organisms offers a third ncAA for studies of
48 anabolic activity (9).

49 BONCAT is therefore able to distinguish anabolically active (or more precisely, protein-
50 synthesizing) cells from dormant cells. Downstream analysis through microscopy or sequencing
51 (often following Fluorescence *In Situ* Hybridization, FISH, or isolation via Fluorescence-
52 Activated Cell Sorting, FACS), enables an array of ecophysiological interpretations. For
53 instance, BONCAT has been used to show carbon use preferences of distinct taxa in hot springs
54 (10) and salt marsh sediment (11), active microbes in the soil microbiome (12) and biocrusts
55 (13), and symbiotic relationships between anaerobic methane-oxidizing archaea (ANME) and
56 sulfate-reducing bacteria in the deep sea (5).

57 Despite the substantial advances made possible by BONCAT in the study of cultured
58 organisms and environmental microbial communities, all known applications of BONCAT to
59 date have used only one ncAA in a given experiment. While this technique has allowed
60 researchers to access the anabolically active subpopulation of a microbial community in a given
61 experimental context, it is not capable of identifying activity patterns among a single population
62 under different or changing conditions. Here, we present a novel approach making use of two
63 ncAAs - AHA and HPG - in a single experiment, a technique we refer to as "dual-BONCAT".
64 This method offers additional versatility for more complex and environmentally representative
65 experimental designs: by selectively labeling two distinct protein subsets, dual-BONCAT
66 provides multiplexing capabilities that enable the labeling and analysis of two protein
67 populations within the same cell or sample. Critically, such experiments would not require
68 parallel incubations that may be subject to small but significant differences in community
69 composition and physicochemical parameters, or may be unobtainable with *in situ* or sample-

70 limited studies. With dual-BONCAT, critical spatial relationships that may dictate differential
71 activity under distinct conditions can be retained and explored. In this study, we first validate the
72 dual-BONCAT approach with *E. coli* cell cultures and an environmental microbial community,
73 and then present a proof-of-concept study differentiating salt marsh sediment communities that
74 are active during the day or night.

75 **Results & Discussion**

76 Reagent & Sample Selection

77 For our two ncAA-dye combinations, we selected the AHA-DBCO dye strain-promoted
78 click reaction and the HPG-Azide dye Cu(I)-catalyzed cycloaddition reaction. These selections
79 minimized the potential for false positive signal that could result from using the HPG-Azide dye
80 and AHA-Alkyne dye pairings: the Cu-catalyzed "click" reaction links azide and alkyne groups,
81 meaning unbound azide and alkyne dyes could react with each other and may be more difficult to
82 wash away. The DBCO dye molecule does not contain a reactive alkyne group and would thus
83 not be susceptible to such dye-dye cross-reactions. (The potential for false negative signal is
84 considered below.)

85 We performed our optimization and experimental procedures on cell cultures
86 (*Escherichia coli*) as well as an environmental system hosting a complex microbial community
87 (surface sediment from the Little Sippewissett Salt Marsh on Cape Cod, MA). In this way, we
88 show the efficacy of the dual-BONCAT technique in a well-constrained pure culture context,
89 while also demonstrating the relevance of the technique (as well as the associated challenges)
90 when used with environmental microbiomes.

91 Dual-BONCAT Validation with *E. coli* Cultures

92 To evaluate the effectiveness of various ncAA and dye concentrations for subsequent use
93 in dual-BONCAT experiments, we first conducted a range of mono-BONCAT tests using a
94 single ncAA-dye pairing. Based on previously published research in both cultures and
95 environmental systems (5, 14, 15), we tested a range of ncAA (0-50 μM HPG; 0-500 μM AHA)
96 and dye (0.1-100 μM for both Azide-Cy3 and DBCO-Cy5) concentrations. In *E. coli* cultures,
97 we found that the fluorescence signals from ncAA concentrations ≥5 μM and dye concentrations
98 ≥1 μM were distinguishable from both ncAA-free and cross-reaction (i.e., AHA-Azide-Cy3 and
99 HPG-DBCO-Cy5) control conditions under our chosen microscope settings (Figs. S1-S3). ncAA
100 concentrations of at least 5 μM and dye concentrations of 25 or 100 μM produced particularly
101 strong signals with median fluorescence intensities 12-64 times greater than the corresponding
102 ncAA-free controls (Fig. S3).
103 To validate the dual-BONCAT approach, we conducted a series of experiments with *E.*
104 *coli* cultures using 5 μM HPG, 5 μM AHA, 25 μM Azide-Cy3, and 25 μM DBCO-Cy5, based on
105 our mono-BONCAT results. (Some conditions of higher ncAA and dye concentrations produced
106 marginally higher fluorescence signals, but we prioritized the lower concentrations to minimize
107 costs and avoid potential toxic effects of higher ncAA concentrations (16, 17).) 100 μL of
108 stationary phase culture was added to 9.9 mL of sterile M9 medium; the first ncAA (ncAA#1)
109 was added at inoculation (0h) and the second (ncAA#2), when relevant, was added after 8h of
110 growth at 37 °C. Cultures were fixed after 24h of incubation. We tested several different
111 experimental configurations to determine whether the fluorescence signals from the two different
112 ncAAs were equivalent, and whether the order of ncAA addition and/or the order of post-fixation
113 dye reactions affected the fluorescence intensities.

114 Overall, fluorescence signal from both ncAAs was clearly distinguishable from
115 background and non-specific binding effects regardless of the timing and order of ncAA addition
116 and the order of the dye reactions (Figs. S4-S5, 1). However, we broadly observed higher
117 fluorescence when the HPG-Azide-Cy3 reaction was performed first, as the median Cy3
118 fluorescence was 32% brighter ($p < 0.001$) and the median Cy5 fluorescence was 151% brighter
119 ($p < 0.001$) relative to when the AHA-DBCO-Cy5 was performed first (Fig. 1). This trend
120 included higher intensities associated with non-specific binding effects (e.g., cases where the
121 corresponding ncAA was absent, as in ncAA-free and mono-BONCAT cross-reaction controls),
122 but the overall ability to distinguish true positives from false positives was largely unaffected by
123 the order of the dye reactions: false positives could only explain 1.6% of the true positive (e.g.
124 mono-labelled) data, at most, regardless of dye order. Initially, we had hypothesized that false
125 negatives could result from performing the HPG-Azide reaction first, as the alkyne-azide click
126 reaction could in theory link AHA azide groups with HPG alkyne groups, thereby blocking dye
127 molecules from binding to their corresponding ncAAs and diminishing overall signals. The fact
128 that we did not observe a decrease in fluorescent signal when the HPG-Azide-Cy3 reaction was
129 done first suggests that the AHA-HPG reaction is not favorable - perhaps due to steric hindrance
130 associated with peptide chains - and is not a substantial concern when using the dual-BONCAT
131 approach. Therefore, we recommend performing the HPG-Azide reaction first, and report the
132 results with this dye order unless otherwise specified. Compared with the corresponding mono-
133 BONCAT (mono-stained) controls, the median fluorescence signal of HPG-labeled cells
134 increased (45% increase, $p < 0.001$) when both dye reactions were performed. In contrast, the
135 AHA-associated signal decreased by 48% ($p < 0.001$).

136 In comparing the order of the ncAA addition, Cy3 fluorescence was 13% dimmer ($p <$
137 0.001) but the Cy5 fluorescence was 47% brighter ($p < 0.001$) when HPG was added first
138 relative to when AHA was added first (when the HPG-Azide-Cy3 dye reaction was done first).
139 This trend was repeated when the dye order was switched. This observation that a given ncAA
140 generates brighter signal when added second rather than first is intriguing, and may be due to
141 protein turnover dynamics whereby proteins synthesized earlier break down over time.
142 Compared to the mono-BONCAT (dual-stained) controls, the median fluorescence signal of Cy3
143 and Cy5 decreased by 36% ($p < 0.001$) and 21% ($p < 0.001$), respectively, when both ncAA were
144 added simultaneously.
145 The median HPG-Azide-Cy3 signal in the mono-labeled, dual-dyed experiment was
146 significantly brighter (by 222%, $p < 0.001$) than the AHA-DBCO-Cy5 (mono-labeled, dual-
147 dyed) signal. This relationship was also observed when both ncAAs were added at different
148 times: HPG-Azide-Cy3 signal was 210% ($p < 0.001$) brighter when the Azide-Cy3 dye reaction
149 was performed first, and 462% ($p < 0.001$) brighter when it was performed second (when both
150 orders of ncAA addition were taken into account, in both cases) (Fig. 1). Since fluorescence
151 intensity profiles of mono-BONCAT experiments were broadly similar between HPG and AHA
152 (Fig. S3), these findings suggest that the dynamics change when both ncAAs are present: in such
153 cases, HPG may be more effective than AHA at integrating into newly synthesized proteins,
154 and/or the HPG-Azide click reaction may be favored over the AHA-DBCO reaction.
155 To determine if dual-BONCAT is capable of distinguishing distinct populations that were
156 anabolically active at different stages of an incubation, we looked at "differential labeling"
157 patterns, where some cells were only labeled with Azide-Cy3, some were only labeled with
158 DBCO-Cy5, and some were labeled with both dyes. Because the intensity of BONCAT labelling

159 cannot always be taken as a quantitative indication of anabolic activity (due to, among other
160 factors, distinct proteome compositions, varying rates of ncAA:Met substitutions, and variability
161 in the rate of dye entry into the cell across different species (17–19)), we maintained a binary,
162 "labeled" or "not labeled" approach to interrogate differential labeling. Threshold fluorescence
163 intensity values were set by the maximum intensity, in either channel, of the condition in which
164 no ncAAs were added but dye reactions were performed. Cells whose mean intensity exceeded
165 these values in a given fluorescence channel were considered "labeled" with the corresponding
166 ncAA.

167 We first considered the condition in which both ncAAs were present at the same
168 concentration and for the same duration, reasoning that, in this case, no differential labeling
169 should occur. Indeed, all analyzed cells were dual-labled (Fig. S6, S7). Next, we investigated
170 differential labeling patterns among *E. coli* cells when the ncAAs were added at different times.
171 Single cell-level observations showed clear visual evidence of differential labeling: some cells
172 were exclusively labeled with Azide-Cy3, some were exclusively labeled with DBCO-Cy5, and
173 some were labeled with both fluorescent molecules (Fig. 2). Some cells were labeled with neither
174 dye, suggesting they were anabolically inactive during the 24-hour culturing experiment,
175 potentially representing quiescent or dead biomass carried over from the inoculum. Using the
176 threshold-based assessment of labeling, we confirmed that differentially labeled subpopulations
177 were present (Fig. S7). These observations confirm the ability of dual-BONCAT to detect
178 distinct subpopulations that are anabolically active during different phases of an experiment. The
179 fact that the majority of cells in these 24-hour experiments were dual-labeled even when the
180 second ncAA was added eight hours after the first is not surprising given the dynamics of

181 exponential growth in pure culture. Different timelines of adding the ncAAs and terminating the
182 experiment could likely be calibrated to attain a larger proportion of differentially labeled cells.

183 Dual-BONCAT in an Environmental Microbial Community

184 Dual-BONCAT was next deployed with an environmental microbial community, using
185 surface sediment from Little Sippwissett Salt Marsh, which contains a dense and taxonomically
186 and metabolically diverse microbiome (11, 20–23). Our aim was to observe and ultimately
187 characterize the subpopulations of cells that were 1) anabolically active during the 12-hour sunlit
188 day, 2) anabolically active during the 12-hour dark night, 3) anabolically active during both the
189 day and night periods, and 4) not active during the 24-hour experiment. Sediment was recovered
190 from the marsh, returned to the lab, and distributed to mesocosm incubations within several
191 hours. In all experimental conditions, one ncAA was added at dawn (ncAA#1) and the
192 incubation was placed in sunlit conditions; 12 hours later, the incubation was moved to a dark
193 incubator and the second ncAA (ncAA#2) was added. The temperature was maintained at
194 approximately 25 °C throughout.

195 Three ncAA concentration profiles were tested: 5 µM HPG & 5 µM AHA & (referred to
196 as 5/5 below); 50 µM HPG & 50 µM AHA (50/50); and 50 µM HPG & 500 µM AHA (50/500).
197 These conditions expand beyond the ncAA concentrations optimized for *E. coli* (5 µM for each
198 ncAA) in order to match HPG concentrations previously optimized for LSSM sediment (11, 22),
199 and to account for the fact that AHA is sensitive to reduction under alkaline sulfidic conditions
200 such as those in Little Sippewissett salt marsh sediments (14), meaning that its "felt"
201 concentration was likely lower than what was added. All dye concentrations were maintained at
202 25 µM based on the *E. coli* optimization experiments described above.

While fluorescence signal derived from HPG incorporation was substantially brighter than that from AHA incorporation across all conditions when their concentrations were equal, both ncAAs were statistically distinguishable from background and non-specific binding effects under elevated ncAA conditions (e.g., the 50/50 and 50/500 experiments; Figs. 3; S8-S9). (The p-values were < 0.001 for all ncAA combinations except for the Cy5 signal when both ncAAs were added at the start of the 50/50 experiment, $p = 0.052$, though cells brighter than the non-specific binding signal were detected.) The 5/5 condition resulted in fluorescence signals that were largely indistinguishable from background and non-specific binding signals (Fig. S10). Prior to click-chemistry reactions, cells from the LSSM sediment incubations were extracted to separate them from the mineral matrix. Compared with *E. coli* culture experiments run under analogous ncAA concentrations, median fluorescence intensity of *E. coli* cells subjected to the cell extraction process decreased by 18% ($p < 0.001$) and 54% ($p < 0.001$) for Cy3 and Cy5, respectively, indicating that the extraction approach itself compromised signal intensity (but not detectability compared with control treatments). Under the 50/50 condition, the median fluorescence signal of labeled sediment cells decreased by 47% ($p < 0.001$) for Cy3 and 54% ($p < 0.001$) for Cy5 when both ncAAs were added simultaneously, compared with their mono-BONCAT (dual-stained) controls (Fig. 3A). In contrast, Cy3 increased by 27% (not statistically significant, $p = 0.34$) and Cy5 increased by 106% ($p < 0.001$) in the 50/500 experiment (Fig. 3B).

In comparing the order of ncAA addition for the 50/50 experiment, Cy3 fluorescence was 248% brighter ($p < 0.001$) but the Cy5 fluorescence was 28% dimmer ($p < 0.05$) when HPG was added first relative to when AHA was added first (and HPG-Azide-Cy3 dye reaction was performed first in both cases). This trend was repeated when the dye order was switched, and, in

226 contrast to the *E. coli* experiments, indicates that a given ncAA generates brighter signal when
227 added first, potentially due to slower protein turnover or degradation in the environmental
228 community compared with a pure culture.

229 In all four dual-BONCAT permutations (testing the order of ncAA additions and dye
230 reactions) with the 50/50 experiment, the HPG-Azide-Cy3 signal was generally brighter than the
231 AHA-DBCO-Cy5 signal. This was also observed when both ncAAs were added: HPG-Azide-
232 Cy3 signal was 432% ($p < 0.001$) brighter when the Azide-Cy3 dye reaction was performed first,
233 and 166% ($p < 0.001$) brighter when it was performed second. These patterns are broadly
234 improved (i.e., the AHA-DBCO-Cy5 signal is generally brighter) under the 50/500 condition,
235 indicating that relative concentrations of the ncAAs, even under sulfidic conditions, can be used
236 to "tune" detectability and relative signal intensities.

237 Experiments in which AHA was added first (at sunrise) and HPG was added second (at
238 night) resulted in a greater overall separation of fluorescent signal compared with control
239 conditions, offering the best opportunity to detect cells growing at different times.

240 We next considered differential labeling patterns at the single-cell level. When both
241 ncAAs were added at the start of the experiment, nearly all cells were dual-labeled (Fig. S11).
242 When one ncAA was added at sunrise and the other at sunset, we observed distinct
243 subpopulations of cells exhibiting only HPG-Azide-Cy3, only AHA-DBCO-Cy5, both dyes, and
244 neither dye (Fig. 4).

245 <u>Interpretation of Dual-BONCAT Subpopulations</u>

246 Interpreting the physiological / ecological meaning of the three differentially labeled cell
247 populations is not entirely unambiguous. Dual-BONCAT experiments can be generalized as
248 follows: one ncAA (ncAA#1) is added at an initial time point (T_1), a second ncAA (ncAA#2) is
249 added at a subsequent time point (T_2), and the experiment is ended (i.e., all metabolic activity is
250 ceased) at a later, final time point (T_F); see Fig. S12. The three differentially BONCAT-labeled
251 populations can be identified as the cells exhibiting fluorescence associated with only the first
252 ncAA (ncAA#1), both ncAAs (ncAA#1&2), and only the second ncAA (ncAA#2). We propose
253 the following interpretations of these three populations:

254 - The ncAA#1 population is only active between T_1 and T_2.
255 - The ncAA#1&2 population includes cells that either are active from both T_1 to T_2 *and* T_2
256 to T_F, or are active between T_2 and T_F. Because ncAA#1 could be present throughout the
257 experiment, it could still be used by organisms exclusively active after T_2. Such dual-
258 labeled cells may exhibit a particularly high affinity for ncAA#1.
259 - The ncAA#2 population is only active between T_2 and T_F. We suggest that the lack of
260 ncAA#1 incorporation in this population could be due to the relative ncAA
261 concentrations during the second phase of the experiment, after the ncAA#1 pool has
262 been depleted. If these cells were anabolically active when only ncAA#1 was present, it
263 would have been incorporated.

264 These interpretations are predicated on previous observations that all taxa queried to date are
265 capable of using each of the two ncAAs at roughly equivalent incorporation frequencies ((17)
266 and references therein). If these frequencies differ between the two ncAAs, further calibration of
267 concentrations would be needed to attain similar fluorescence signals. (For reference, HPG and
268 AHA replace an estimated 1 out of every 500 and 390 methionine residues in newly synthesized

269 proteins, respectively (24), while the newly reported THRONCAT approach has a substitution
270 efficiency of 1:40 (9).)

271 Dual-BONCAT-FACS Reveals Day- and Night-Active Taxa in Salt Marsh Sediment

272 To demonstrate the utility of the Dual-BONCAT technique for studying the dynamics of
273 environmental microbial communities, we sought to identify which microbes in salt marsh
274 sediment were active (synthesizing proteins) during sunlit daytime hours and which were active
275 during nighttime darkness. Critically, this approach did not require separate incubations, which
276 obviates concerns about distinct microbial communities or physicochemical conditions across
277 supposed "replicate" samples.

278 Two lab-based experimental incubations of shallow (0-3 cm) salt marsh sediment were
279 performed. In Condition 1, HPG was added at sunrise (T_1) and AHA was added 12 hours later
280 (T_2), when the incubation was moved to a dark environment. In Condition 2, the order of ncAA
281 addition was reversed. We also included a negative control treatment that did not receive any
282 ncAAs but did receive both dyes. The downstream use of Fluorescence-Activated Cell Sorting
283 (FACS) requires stained cells to be in suspension rather than affixed to slides, prompting some
284 modifications to the slide-based protocol (detailed in the Materials & Methods section). In
285 particular, we found that 25 μM Azide-Cy3 and 1 μM DBCO-Cy5, when applied to 50 μM
286 concentrations of both ncAAs, was sufficient to differentiate true positive from false positive
287 signal in cell sorting experiments. For both experimental conditions, we confirmed the detection
288 of all three populations of cells (ncAA#1, ncAA#1&2, and ncAA#2) under the microscope prior
289 to cell sorting.

290 The three BONCAT-active populations from each of the two incubations were isolated
291 using FACS, based on gates determined using negative and mono-BONCAT positive controls

292 (Fig. S13). With the exception of the ncAA#2 population (active only at night) from Condition 1,
293 which generated FACS cell counts below the detection limit, between $2.1x10^4$ and $7.2x10^5$ cells
294 were sorted for each population (Table S1). Subsequent high-throughput 16S rRNA gene
295 amplicon sequencing allowed us to compare these distinct populations and infer
296 ecophysiological differences among day- and night-active taxa.

297 Among the taxa that were most prominent within the day-active (ncAA#1) population
298 (Fig. 5; Tables S2, S3), the *Beijerinckiaceae* genus *Methylobacterium* is commonly associated
299 with plants, and can use one-carbon compounds, including methanol in plant exudate, as a
300 carbon source (25, 26). At LSSM, roots of the cordgrass *Spartina alterniflora* permeate the
301 sediment and release a chemically diverse array of organic molecules. Heterotrophs feeding on
302 exudate, such as *Methylobacterium*, were likely stimulated by the *Spartina*'s daytime
303 photosynthetic activity; a similar relationship was observed with nitrogen-fixing microorganisms
304 surrounding *Spartina* roots, whose activity was substantially enhanced within an hour of light
305 exposure (27).

306 Sulfur-cycling taxa were highly abundant members of the night-active community
307 (ncAA#2 population). *Chromatiaceae*, the purple sulfur bacteria that comprise a key constituent
308 of the syntrophic "pink berry" consortia (21), accounted for 14% of the night-active population;
309 while this taxon is photosynthetic, its dark-phase respiration metabolism (28, 29) may be more
310 tightly coupled with protein synthesis. (We are confident that this enrichment was not due to
311 *Chromatiaceae* autofluorescence because signals in ncAA-free control experiments did not rise
312 above the threshold of "positive" detection; Fig. 3). *Arenicellaceae*, whose close relative
313 UBA868 may play a foundational role in marine sulfur oxidation (30), and the sulfate-reducing
314 bacteria family *Desulfobacteraceae* were both preferentially active at night, perhaps responding

315 more favorably than other anaerobic taxa to expanding anoxic zones that accompany nighttime
316 decreases in oxygenic photosynthesis (31). Other abundant taxa, such as the heterotrophic
317 *Anaerolineaceae* and *Cyclobacteriaceae*, did not exhibit night-specific activity patterns; these
318 organisms likely operate independent of diurnal cycles and depend more on ever-present organic
319 matter rather than shifting redox stratification or specific molecules provisioned during light or
320 dark metabolic phases.

321 **Conclusion**

322 Dual-BONCAT offers a new capability for the visualization and identification of
323 differentially active subpopulations within cell cultures and environmental microbiomes. By
324 revealing organisms that are anabolically active under distinct conditions within the same
325 physical environment, novel syntrophic or antagonistic relationships can be queried, and a more
326 realistic understanding of the condition-specific activity of microbial constituents can be
327 attained. We found that, in *E. coli* cultures and a salt marsh sediment microbial community, both
328 AHA and HPG uptake was detectable, and that distinct subpopulations of cells active during
329 different phases of an experiment were distinguishable. The order of ncAA addition did not have
330 a consistent effect on fluorescent intensity, but the order of dye reaction did: overall, performing
331 the HPG-azide click reaction prior to the AHA-DBCO reaction yielded brighter signals.
332 Downstream FACS and high-throughput 16S rRNA gene sequencing of distinct labeled
333 subpopulations allowed for the ecophysiological interpretation of taxa active during the day and
334 during the night, all without disrupting the community or relying on pseudoreplicate
335 experiments.

336 Challenges associated with dual-BONCAT are similar to those associated with mono-
337 BONCAT, and largely relate to optimizing signal-to-noise ratios in environmental microbiomes.

338 Low signal challenges may be accentuated when both ncAAs are present, since competition for
339 Met substitution would be expected to lower incorporation of each ncAA by approximately half.
340 We recommend that users customize ncAA concentrations, dye concentrations, and imaging
341 parameters to optimize for their specific applications, as diffusivity and non-specific binding
342 effects can vary with biofilm density, mineralogical context, and other physicochemical factors.
343 However, given the broad flexibility of mono-BONCAT more generally, we anticipate that the
344 methods and parameters we describe here will be a successful starting point for most
345 applications, including isolate cultures and complex environmental samples.

346 We envision many promising use cases for the dual-BONCAT approach, which allows
347 researchers to interrogate how a specific microbial community responds to changing conditions.
348 For example, the technique could track spatial patterns of protein synthesis within cell aggregates
349 or biofilms, or identify anabolically active taxa, in response to a shift in temperature, pH, redox
350 potential, predation, oxygen concentration, or any other manipulatable variable. Protein pull-
351 down experiments, which capture newly-synthesized proteins for downstream sequencing (32),
352 could incorporate dual-BONCAT to identify sub-proteomes linked with responses to
353 environmental challenges. Because of microscale heterogeneity in microbial community
354 composition (33, 34), "replicate" experiments are often insufficient in these contexts. Using
355 dual-BONCAT to observe the response of a single community as conditions change offers a
356 more realistic, representative view of dynamic microbiomes.

357 **Materials and Methods**

358 Sample Growth & Collection

359 *E. coli* was used first to identify the optimal concentrations of AHA and HPG, along with
360 their conjugate dye concentrations, and second to test dual-BONCAT approaches. The selection

361 of *E. coli* as our experimental organism was based on its rapid replication time, high expression
362 capabilities, and previous utility in BONCAT method development. Given that both non-
363 canonical amino acids used in this study, AHA and HPG (both supplied by Click Chemistry
364 Tools, Scottsdale, AZ), serve as surrogates for methionine, M9 medium, a growth medium that
365 lacks methionine, was used to grow the cultures. *E. coli* was initially inoculated from a glycerol
366 stock into M9 medium and grown overnight. (This *E. coli* stock had been grown in LB nutrient-
367 rich medium prior to being stored in glycerol.) We then took 100 µL of early stationary phase *E.*
368 *coli* culture in M9 to inoculate 9.9 mL of sterile M9 media. The first ncAA was added at the time
369 of inoculation; the second, when relevant, was added at a designated intermediate time point (8
370 hours). All ncAA and dye concentrations are indicated in the main text for each specific
371 experiment.

372 To explore the use of Dual-BONCAT with environmental microbial communities, we
373 used sediment from Little Sippewissett Salt Marsh on Cape Cod, MA, USA. Sediment from 0-3
374 cm depth was collected from the "Berry Pool" (located at 41.5758° latitude, -70.6394°
375 longitude); these sediments contained small *Spartina alternaflora* grasses and are marked by
376 sharp redox gradients with diurnal geochemical shifts, as well as a strong heritage of microbial
377 diversity studies, some of which have successfully deployed BONCAT and BONCAT-FACS-
378 16S techniques (11, 20, 22, 31). Immediately following collection, sediment was returned to the
379 lab and placed next to a large window at room temperature. Incubation experiments began within
380 two days after collection, and ncAAs were added at designated time points from stock solutions
381 to reach the desired final concentrations. AHA is sensitive to reduction under alkaline sulfidic
382 conditions such as those in LSSM sediments (14); thus, the AHA added to the incubations should
383 be viewed as an upper bound on the "felt concentration" within the experiments. Incubations

384 were conducted in 15 mL Falcon tubes with 5 mL of sediment and 5 mL of co-localized marsh
385 water. For day/night dual-BONCAT experiments, ncAA#1 was added at sunrise, and incubations
386 were placed next to a large window with direct daytime light. Twelve hours later, ncAA#2 was
387 added and the incubations were placed in a sealed incubator at room temperature. Controls with
388 no ncAAs, only one ncAA, and both ncAAs added at the start of the experiment were also
389 included. For fluorescence activated cell sorting experiments, control incubations were set up for
390 1) a Cy3 Positive Control (mono-BONCAT with HPG-Azide-Cy3), 2) a Cy5 Positive Control
391 (mono-BONCAT with AHA-DBCO-Cy5), 3) a Cy3&Cy5 Positive Control (both ncAAs added
392 for the full duration of an incubation experiment), and 4) a Negative Control (neither ncAA was
393 added, but Azide-Cy3 and DBCO-Cy5 dyes were). All ncAA and dye concentrations are
394 specified in the text.

395 To stop the incubations at the designated time points, samples were chemically fixed to
396 cease metabolic activity and prepare the cells for click chemistry reactions and imaging. To do
397 this, 0.5 mL aliquots of culture or sediment slurry were placed in sterile 2 mL tubes, and 1.5 mL
398 of 0.22-µm filter sterilized 3% paraformaldehyde in 1x PBS was added to each tube. This
399 mixture was mixed briefly by vortex and kept at room temperature for one hour. The tube was
400 then centrifuged at 8,000 x *g* for 5 minutes and the supernatant was discarded. The pellet was
401 washed twice with 1x PBS (by resuspending in 1 mL of 1x PBS, centrifuging at 8,000 x *g* for 5
402 minutes, and removing the supernatant) and ultimately resuspended in 1 mL of 1:1 PBS:ethanol.
403 The sample was then kept at 4 °C until downstream processing.

404 <u>Cell Extraction from Sediment Samples</u>

405 To recover cells from LSSM sediment and minimize the effects of autofluorescent
406 mineral grains, a cell extraction was performed following a protocol established by Couradeau et

407 al. for the soil microbiome (12) and successfully used in LSSM sediment (11). Fixed sediment
408 was centrifuged at 5,000 x *g* for 3 minutes, the supernatant was removed, and ~250 µL of
409 sediment (or fixed culture, for controls) was transferred to a new 2 mL tube. 1450 µL of sterile
410 1x PBS and 34.7 µL of sterile 1% Tween20 were added to the tube, which was then inverted
411 several times and vortexed at maximum speed for 5 minutes to thoroughly mix the sample and
412 promote the removal of cells from sediment grains. Tubes were then centrifuged at 500 x *g* for
413 55 minutes to separate cells (into the supernatant) from sediment (which formed a pellet). The
414 supernatant was then transferred to a new 2 mL tube, being sure to avoid any sediment.
415 A second extraction of the initial sediment was then performed by adding 870 µL of
416 sterile 1x PBS and 20.8 µL of sterile 1% Tween20 to the tube containing the sediment. The tube
417 was inverted several times, vortexed at maximum speed for 5 minutes, and centrifuged at 500 x *g*
418 for 35 minutes. The supernatant was then recovered and pooled with the previously collected
419 supernatant from the first extraction. The pooled extraction product was then centrifuged at
420 16,000 x *g* for 6 minutes to pellet the cells. The supernatant was discarded and the pellet was
421 resuspended in 250 µL of 1:1 PBS:ethanol. These fixed, extracted cells were then used for
422 downstream cell staining analyses.
423 <u>Cell Staining with Click Chemistry for Microscopy</u>
424 10 µL of fixed cells were added to a single well of a slide (Tekdon slides 8-82 with
425 Teflon and poly-L-lysine coating) and dried at room temperature. To dehydrate and permeabilize
426 the cells, 10 µL of 50%, 80%, and 96% ethanol were sequentially added to each well for at least
427 3 minutes each, and dried at room temperature in between. (A gentle stream of filtered
428 pressurized air can be used to accelerate the drying process.) We found that performing the

429 dehydration and click chemistry reactions directly on the wells rather than submerging the entire
430 slide in coplin jars reduced cross-contamination between wells.

431 The click chemistry reactions described below can be done either in isolation (e.g., AHA-
432 DBCO or HPG-azide for a "mono-BONCAT" application) or in series for dual-BONCAT. While
433 we initially thought performing the AHA-DBCO reaction first would be best in order to avoid
434 potential false negatives from AHA azides reacting with HPG alkynes, assessment of the
435 resulting signal suggests this effect may be negligible. Instead, we recommend performing the
436 HPG-Azide reaction first as this order of operations retained a brighter Cy5 fluorescence from
437 the AHA-DBCO signal.

438 *HPG-Azide Reaction*

439 To perform the Cu(I)-catalyzed HPG-azide reaction, we first made two "premix"
440 solutions in separate 2 mL tubes according to Table S4. (All volumes mentioned here can be
441 adjusted proportionally based on the number of samples and volume of dye mix needed to fully
442 cover the analyte cells, as well as the desired dye concentration; the volumes listed here assume a
443 25 µM final dye concentration and 20 µL of dye mixture applied to each microscope slide well.)
444 Premix 1 contained the 100 mM solutions of Na-ascorbate and aminoguanidine-HCl (both in 1x
445 PBS; solutions made fresh on the day of use), as well as the 1x PBS. Premix 2 contained the 20
446 mM $CuSO_4$, 50 mM Tris-HydroxyPropylTriazolylmethylAmine (THPTA), and concentrated (1
447 mM) azide dye (Cy3 picolyl azide dye, Click Chemistry Tools, Scottsdale, AZ); these
448 components were left to incubate in the dark at room temperature for 3 minutes. The final dye
449 concentration can be adjusted based on the volume and concentration of the dye stock solution
450 used; overall volume can be maintained by adjusting the amount of 1x PBS. The two premixes
451 were then combined and inverted once to mix gently.

452 The incubation of cells with the dye mixture was performed in a humid chamber
453 consisting of a 50 mL Falcon tube placed on its side, with ultrapure water- or 1x PBS-saturated
454 kimwipes inside. 20 µL of dye mixture was applied to each slide well, and the slide was carefully
455 inserted into the humid chamber, making sure the lens of liquid remained intact on top of each
456 well. The humid chamber was then capped and placed in the dark at 46 ^{o}C for 30 minutes.
457 Following the incubation, the dye was removed by carefully pipetting the solution off from the
458 edge of the well (so as to not disturb the cells in the center) and rinsing each well three times
459 with 20 µL of 1x PBS (applied and removed by pipette). Finally, the slide was dehydrated with
460 10 uL of 50% ethanol in 1x PBS for 3 minutes and then dried under a gentle stream of
461 pressurized air.

462 *AHA-DBCO Reaction*

463 To perform the strain-promoted AHA-DBCO reaction, 20 µL of fresh 100 mM 2-
464 chloroacetamide (in 1x PBS) were added to each slide well and incubated in the humid chamber
465 for 1 hour at 46°C. A dye mix was made with concentrated DBCO-Cy5 dye (Click Chemistry
466 Tools, Scottsdale, AZ) and the chloroacetamide solution; the volume and concentration should
467 be adjusted to attain the desired final concentration (previously recommended to be between 100
468 nM – 1 µM (14)). We found a final dye concentration of 25 µM to work best for *E. coli*, so we
469 used this concentration for the salt marsh sediment samples as well. The chloroacetamide was
470 removed and 20 µL of the DBCO-Cy5 dye mix was added to each well. Slides were left to
471 incubate in the humid chamber for 30 minutes at 46 ^{o}C in the dark. Unbound dye was removed
472 by adding 20 µL of 1:1 dimethyl sulfoxide:PBS to each slide well and incubating in a humid
473 chamber at room temperature for 20 minutes. Wells were then rinsed three times with 20 uL of

474 1x PBS. Finally, the slide wells were dehydrated with 10 uL of 50% ethanol in 1x PBS for 3
475 minutes and then dried under a gentle stream of pressurized air.

476 *DAPI Counterstaining*

477 To visualize all cells - and thereby confirm that BONCAT signals corresponded with
478 biomass while also allowing for cell abundance calculations - the general DNA stain 4',6-
479 diamidino-2-phenylindole (DAPI) was used. For each well, 6 µL of a 1:1 mixture of 5 ng/µL
480 DAPI:VectaShield Antifade Mounting Medium was added and spread across each well by
481 adding a glass coverslip.

482 Fluorescence Microscopy

483 Microscopic analysis was performed on a Leica Stellaris 5 confocal laser scanning
484 fluorescence microscope equipped with a white light laser and tunable excitation wavelengths
485 and emission windows. For all imaging, a 63x immersion objective lens was used and carried out
486 in the Leica Application Suite X (LAS-X). Imaging parameters for all dyes and both cell culture
487 and environmental samples are provided in Table S5. All imaging parameters were kept constant
488 for experimental and control treatments in order to provide directly comparable data sets (with
489 the exception of the DAPI detector gain, as the sediments were overexposed when the gain was
490 set to 8%). We also found that there was substantial reflection when the detector emission
491 window was <15 nm away from the laser excitation, which is why we deviated from the default
492 settings in LAS-X. For each field of view, three images - corresponding to all cells (DAPI), all
493 AHA-incorporating cells (Cy5), and all HPG-incorporating cells (Cy3) - were acquired and
494 analyzed in parallel.

495 Image Analysis

496 Images were analyzed using FIJI / ImageJ version 2.14.0/1.54f (35). Composite and
497 individual channel images were generated and brightness was adjusted uniformly using our FIJI-
498 Multi-Channel-RGB-Stacker plugin (https://github.com/mankeldy/FIJI-Multi-Channel-RGB-
499 Stacker) with the settings in Table S6. Cell-specific fluorescence intensity data was extracted
500 using our FIJI-Multi-Channel-Cell-Counter plugin (https://github.com/mankeldy/FIJI-Multi-
501 Channel-Cell-Counter) with the settings in Table S7. Initially, we noticed our DAPI images were
502 slightly offset (roughly 0.25 μm) from our Cy3 and Cy5 images, so we used the MultiStackReg
503 (v1.46.5) plugin to apply a rigid-body transformation that aligned the Cy3 and Cy5 images to the
504 corresponding DAPI image in a representative field of view. Transformations were applied
505 across all fields of view in each experiment, and both the *E. coli* and sediment experiments used
506 dual-labelled *E. coli* as the reference for extracting the transformation matrix. Next, for *E. coli*,
507 we used the DAPI channel as our reference to find ROIs after applying the Moments automatic
508 threshold, and we only selected those ROIs that had areas between 0.1-2 μm^2. These ROIs were
509 then redirected onto the corresponding raw DAPI, Cy3, and Cy5 images to extract the mean cell-
510 specific intensity across each channel. For the salt marsh sediments, we chose to use the Cy3 and
511 Cy5 channels (with a Moments threshold) as our reference to find ROIs, since the diffuse DAPI
512 background in many of these images would lead to false positives/negatives with automated
513 thresholding methods. We subsequently applied a Watershed (tolerance: 0.5) to separate
514 overlapping cells and kept ROIs with areas between 0.1-4 μm^2 and a circularity between 0.2-1.
515 Normalizing the cell-specific fluorescence in each channel by the corresponding DAPI signal is
516 often useful to account for slight variations in intensity for cells on the edge of the focal plane.
517 However, the cell-specific DAPI fluorescence varied dramatically in the salt marsh sediments
518 (likely due to species-specific variations in GC content (36, 37); genome size, substrate

519 limitation, growth stage, and number of genome copies (38); and permeability (39, 40)), leading
520 to unreliable "normalized" intensities. (These factors also precluded an analysis of Cy3:Cy5
521 ratios for confirmed DAPI-active cells comparable to that conducted for *E. coli* cells, e.g., Fig.
522 S7.) Therefore, we report the raw mean cell-specific intensities for all analyses, which remain
523 comparable across experiments since the same imaging parameters were used throughout the
524 study (Figs. 1, 3, S3, S10). To identify differentially labelled cells, we considered only those
525 cells whose mean intensities in either the Cy3 or Cy5 channels were greater than the ncAA-free
526 (but dyed) controls as being labelled with the corresponding ncAA. For a given cell, if both
527 intensities were greater than the ncAA-free condition, then it was considered "dual-labelled."
528 Otherwise, it was either "only HPG" or "only AHA" labelled (Fig. S7).
529 All plots in this study were made using ggplot2 (v3.4.4
530 https://doi.org/10.32614/CRAN.package.ggplot2). Statistical significance was determined using
531 the Whitney-Mann *U* test (R function *wilcox.test*). False positives rates in the dual-BONCAT
532 validation experiments were calculated based on the portion of cells in the mono-labelled
533 controls that were dimmer than the maximum mean cell fluorescence in either the ncAA-free or
534 opposite mono-labelled controls, depending on which was greater. Additional packages used for
535 data formatting and plotting include the following:
536 dplyr (v1.1.4 https://doi.org/10.32614/CRAN.package.dplyr)
537 reshape2 (v1.4.4 https://doi.org/10.32614/CRAN.package.reshape2)
538 stringr (v1.5.0 https://doi.org/10.32614/CRAN.package.stringr)
539 extrafont (v0.19 https://doi.org/10.32614/CRAN.package.extrafont)
540 scales (v1.2.1 https://doi.org/10.32614/CRAN.package.scales)
541 tidyr (v1.3.1 https://doi.org/10.32614/CRAN.package.tidyr)

542 rstudioapi (v0.17.1 https://doi.org/10.32614/CRAN.package.rstudioapi)

543 gg4hx (v0.3.1.9000 https://doi.org/10.32614/CRAN.package.ggh4x)

544 forcats (v1.0.1 https://doi.org/10.32614/CRAN.package.forcats)

545 Fluorescence-Activated Cell Sorting

546 *BONCAT Protocol Modifications for FACS*

547 Because FACS requires stained cells to be in suspension, some modifications to the slide-
548 based protocol described above were implemented. Starting from fixed cells in a 1:1 solution of
549 PBS:ethanol, a 5-minute centrifugation at 16,000 x *g* was performed to pellet the cells, and the
550 supernatant was discarded. The cells were resuspended in 250 µL of 80% ethanol, vortexed, and
551 incubated at room temperature for 3 minutes. Next, 1.5 mL of 96% ethanol was added to the
552 tube, which was then vortexed and left at room temperature for 3 minutes. The sample was
553 centrifuged at 16,000 x *g* for 5 minutes, the supernatant was removed, and the pellet was
554 resuspended in 221 µL of 1x PBS. The cells were pelleted again (16,000 x *g* for 5 minutes,
555 supernatant removed) and resuspended in 500 µL of 100 mM 2-chloroacetamide in 1x PBS, and
556 incubated for 1 hour in the dark. To stain the azide AHA molecules, DBCO-Cy5 was added to
557 reach the desired final concentration (1 µM for cells extracted from salt marsh sediment to be
558 used for FACS), and the sample was incubated in the dark at 46 ºC for 30 minutes. Following the
559 incubation, the sample was washed three times with PBS and once with 50% ethanol in 1x PBS;
560 each wash involved centrifuging at 16,000 x *g* for 5 minutes, removing the supernatant, and
561 resuspending cells in wash fluid. After the final wash step, the sample was resuspended in 500
562 µL of 1x PBS solution containing the desired concentration of the azide-Cy3 dye (25 µM, in this
563 case). The tube was inverted once to gently mix, and the sample was left to incubate in the dark
564 at room temperature for 30 minutes. To remove any unbound dye, the sample was then washed

565 three times with 1x PBS and once with 50% ethanol in 1x PBS; each wash involved centrifuging
566 at 16,000 x *g* for 5 minutes, removing the supernatant, and resuspending cells in wash fluid.
567 Finally, the cells were resuspended in a 1:1 solution of PBS:ethanol and kept at -20 ºC prior to
568 loading onto the FACS instrument. For microscopic confirmation of staining, a few microliters
569 can be placed on a slide and counterstained with DAPI, as described above.

570 *Cell Sorting Procedures*

571 Six samples of extracted salt marsh sediment microbial communities were sent to the
572 University of Arizona for fluorescence-activated cell sorting (FACS): Condition 1 (ncAA#1:
573 HPG-azide-Cy3; ncAA#2: AHA-DBCO-Cy5); Condition 2 (ncAA#1: AHA-DBCO-Cy5;
574 ncAA#2: HPG-azide-Cy3); Cy3 Positive Control (mono-BONCAT with HPG-azide-Cy3); Cy5
575 Positive Control (mono-BONCAT with AHA-DBCO-Cy5); Cy3&Cy5 Positive Control (both
576 ncAAs added for the full duration of an incubation experiment); and Negative Control (neither
577 ncAA was added, but azide-Cy3 and DBCO-Cy5 dyes were). A BD Influx flow cytometer (BD
578 Life Sciences, USA) was used to isolate cells from distinct gated subpopulations by FACS. The
579 instrument fluidic system was thoroughly cleaned before use with multiple rinses of 10% bleach,
580 70% ethanol, and ultrapure water (8). The sheath fluid consisted of 1x PBS filtered through a
581 0.2-µm filter and autoclaved at 121°C for 30 min (hereafter referred to as sterile). The sheath
582 fluid was also filtered through a 0.2-µm Sterivex filter (FisherScientific catalog #SVGPL10RC)
583 connected in line with the sheath tank. A 70-µm nozzle was used, with a sheath fluid pressure of
584 30 PSI (207 kPa) and a sample fluid pressure of 31 PSI (214 kPa). The instrument was aligned,
585 focused, and calibrated using reference microspheres (1-µm Fluoresbrite Multifluorescent,
586 Polysciences catalog #24062; and 3-µm Ultra Rainbow, Spherotech catalog #URFP-30-2).

587 Samples were vortexed and filtered onto a BD Falcon 40-µm nylon cell strainer (BD
588 Biosciences, catalog #352340) into polypropylene disposable tubes (BD Biosciences, catalog
589 #352063) to avoid clogging the nozzle with cell clumps. To identify populations of interest, cell
590 doublets were initially excluded using a trigger pulse width versus forward scatter plot. This
591 approach assumes that pulse width typically covaries with forward scatter for single particles;
592 doublets exhibit comparable forward scatter to single cells but have an increased pulse width.
593 Consequently, total events were gated to include only those with similar pulse width to forward
594 scatter ratios in the analyses (Fig. S13). A scatter plot displaying 585/29 nm emission at 561 nm
595 excitation versus forward scatter was used to detect Cy3 labeled cells (hereafter referred to as the
596 Cy3 plot), while a scatter plot featuring 692/40 nm emission at 640 nm excitation versus forward
597 scatter detected Cy5 labeled cells (hereafter called the Cy5 plot). Another scatter plot was
598 generated to detect Cy3&Cy5 dual-labeled cells (hereafter called the Cy3&Cy5 plot),
599 showcasing 692/40 nm emission at 640 nm excitation (Cy5) versus 585/29 nm emission at 561
600 nm excitation (Cy3). Negative controls consisting of ncAA-free samples with Cy3, Cy5, or Cy3
601 and Cy5 dyes were used to draw the background gates on the Cy3, Cy5, and Cy3&Cy5 plots.
602 Cy3 and Cy5 mono-labeled control samples were analyzed to determine the background signal
603 generated in the Cy5 and Cy3 plots, respectively (i.e., to determine fluorescence bleed-through),
604 and to draw the Cy3-positive and Cy5-positive subpopulation gates. Cy3&Cy5 dual-labeled
605 control samples were analyzed to draw the Cy3&Cy5-positive gate on the Cy3&Cy5 plot.
606 At the beginning of each sample processing day, the drop delay was calibrated using BD
607 FACS Accudrop Beads (catalog #345249). The sorting efficiency was manually verified by
608 sorting a designated number of 1-µm Fluoresbrite yellow-green microspheres (Polysciences
609 catalog #17154-10) onto a glass slide, followed by counting the beads under an epifluorescence

610 microscope. The breakoff position was monitored throughout the day and adjusted as necessary.
611 The instrument was set to high sorting purity (1.0 drop) mode. To maintain high sorting purity
612 and recovery, samples were diluted in sterile 1x PBS as needed to achieve an event rate of less
613 than 5,000 per second, thereby avoiding coincidence and swarm (41). Cells from each sorted
614 subpopulation were collected into separate sterile microtubes. After collection, samples were
615 stored frozen at -80°C. The number of sorted cells recovered using the approaches described
616 above is provided in Table S1.

617 16S rRNA Gene Sequencing & Analysis

618 *DNA Extraction & Sequencing*

619 DNA was extracted from the FACS-sorted samples by a modified hot phenol/chloroform
620 extraction (42, 43). All reagents were molecular grade and nuclease-free. Sorted samples were
621 added to Invitrogen Bead Tubes (Thermo Fisher #A29158) with 500 µL of extraction buffer
622 (10% (w/v) CTAB buffer at pH 8, 100 mM Tris-HCl, 100 mM Na-EDTA, 100 mM NaH_2PO_4,
623 1.5 M NaCl) heated to 75ºC (for easier transfers). Bead tubes were vortexed for 5 minutes and
624 inverted periodically to ensure proper mixing. 50 µL of 50 mg/mL lysozyme and 10 µL of 20
625 mg/mL Proteinase K were added to each tube and incubated at 37 ºC for 30 minutes. After
626 incubation, 210 µL of 20% (w/v) sodium dodecyl sulfate (SDS) were added to each bead tube
627 and incubated for 2 hours at 65 ºC. Tubes were then centrifuged at 10,000 x *g* for 10 minutes and
628 the supernatant was transferred to a 2 mL Eppendorf tube and placed on ice. A second extraction
629 was performed by adding an additional 500 µL of extraction buffer to the original bead tubes.
630 Bead tubes were vortexed for another 10 minutes and inverted periodically. Another 70 µL 20%
631 (w/v) SDS was added and tubes were incubated at 65 ºC for 1 hour. Bead tubes were centrifuged
632 at 10,000 x *g* for 10 minutes, and the remaining supernatants were combined with the first

633 extractions. An equal volume of 60 ºC (pre-heated) phenol:chloroform:isoamyl alcohol (25:24:1,
634 adjusted to pH 7.9 with Tris buffer) was added to each extract and inverted gently to mix. Tubes
635 were centrifuged at 13,800 x *g* for 30 minutes, and the upper aqueous layer was transferred into a
636 fresh 1.5 mL Eppendorf tube. To precipitate the DNA, approximately 0.6 extract volume's worth
637 of isopropyl alcohol and 0.6 volume's worth of 0.3 M Na-Acetate (pH 5.2) were added to each
638 Eppendorf tube and inverted gently to mix. Tubes were placed at 4 ºC and allowed to precipitate
639 overnight. Tubes were centrifuged at 16,000 x *g* for 20 minutes, and the supernatant was
640 discarded. DNA pellets were washed with ~200-500 µL of chilled 75% ethanol and centrifuged
641 for another 16,000 x *g* for 10 minutes. The supernatant was discarded and the remaining DNA
642 pellets were allowed to air dry for 15-30 minutes. DNA was resuspended in 50 µL of nuclease-
643 free water and stored at -20 ºC. DNA was quantified on a Qubit 4 Fluorometer (Invitrogen)
644 following the manufacturer's instructions.

645 Extracted DNA was sent to the University of Delaware DNA Sequencing and
646 Genotyping Center for library preparation and sequencing. Initially, some samples did not
647 generate a library, so all samples were cleaned using a Zymo Clean & Concentrator-5 kit. The
648 V4 region of the 16S rRNA gene was amplified based on the Earth Microbiome protocol (44)
649 with the revised 515 F (5'-GTGYCAGCMGCCGCGGTAA-3'; (45)) and 806 R (5'-
650 GGACTACNVGGGTWTCTAAT-3'; (46)) primers for 30 cycles and sequenced on an Illumina
651 MiSeq 251-cycle paired-end run (2x251) with an output of 2M paired reads (analyses only
652 performed on the forward reads, see below). Two controls were included in the sequencing run: a
653 "DNA Extraction Negative Control" that followed the extraction procedure detailed above but
654 included no template, and a "UDel Sequencing Negative Control" that resulted from running 31
655 µL H_2O through the clean and concentrate column and using it as the PCR negative control.

656 *Sequence Analysis*

657 Raw sequence reads were processed on the Boston University Shared Computing Cluster
658 using the BU16s pipeline (https://github.com/Boston-University-Microbiome-Initiative/BU16s)
659 built with QIIME 2020.2 (47) as described in (48) and (49). Sequencing adaptors were removed
660 with cutadapt (50) and amplicon sequence variants (ASVs) were generated with dada2 (51). For
661 taxonomic association, ASVs were clustered to 99% identity with the SILVA 132 database (52)
662 using the vsearch *cluster-features-closed-reference* (53). Initially, reads were analyzed as paired-
663 ends, but this led to few reads passing through the quality filter. Poor reverse read quality was
664 confirmed with FastQC, and the forward reads were processed as a single-end library for
665 subsequent analyses. Raw sequence reads have been archived at the National Centre for
666 Biotechnology Information GenBank under the Bioproject ID PRJNA1188625.

667 ASV analyses were performed with R (v4.3.1) in RStudio (v2023.09.1+494). Alpha
668 diversity metrics were calculated as described in (11) and are provided in Table S8. Data was
669 formatted using Phyloseq (v1.46.0; (54)); to compare samples with uneven sequencing depth,
670 ASVs were rarefied with GUniFrac (v1.8 https://doi.org/10.32614/CRAN.package.GUniFrac).
671 Species richness (Chao and Abundance-based Coverage Estimator (ACE) metrics) and the
672 Shannon diversity index were calculated by Vegan using the *estimateR* and *diversity* functions,
673 respectively (v2.6-10 https://doi.org/10.32614/CRAN.package.vegan). Evenness was determined
674 by dividing the Shannon diversity index by the natural-logarithm of the number of observed
675 ASVs.

676 Relative abundances were calculated by dividing the number of reads from each ASV by
677 the total number of reads in each sample (Table S3). Ambiguous taxonomic classifications (e.g.
678 uncultured, unidentified etc.) were removed from each ASV up to the lowest defined category.

679 For family-level analyses, ASVs were grouped at the family level (or their lowest defined
680 taxonomic label) and relative abundances within each family-level grouping were summed
681 together. If the family was not known, the remaining ASVs were grouped by their order, and so
682 on, moving further up the taxonomic ladder until the domainless ASVs were grouped (Table S2).
683 Of this data, we considered the grouped taxa which accounted for >1% relative abundance in at
684 least one of the conditions (Fig. 5; Table S2). The mean and standard deviation of the Day-active
685 (ncAA#1) and Day- and Night-active or Night-active (ncAA#1 & #2) families were calculated
686 from the two experimental conditions and plotted alongside the Night-active (ncAA#2) families
687 from Condition 2 using ggplot2 (v3.4.4 https://doi.org/10.32614/CRAN.package.ggplot2) (Fig.
688 5). Additional packages used for data formatting and plotting include the following:

689 dplyr (v1.1.3 https://doi.org/10.32614/CRAN.package.dplyr)
690 reshape2 (v1.4.4 https://doi.org/10.32614/CRAN.package.reshape2)
691 stringr (v1.5.0 https://doi.org/10.32614/CRAN.package.stringr)
692 extrafont (v0.19 https://doi.org/10.32614/CRAN.package.extrafont)
693 scales (v1.2.1 https://doi.org/10.32614/CRAN.package.scales)

694 Data Availability

695 All datasets generated during and/or analyzed during the current study are available from
696 the corresponding author upon reasonable request. Raw sequence reads have been archived at the
697 National Centre for Biotechnology Information GenBank under the Bioproject ID
698 PRJNA1188625.

699 **Acknowledgments**

700 We would like to thank Paul Bae and Theodore Dowd for assisting with lab procedures;
701 Claire Andrade, Erin Frates, Jiayi Li, Vinitra Nathan, Dr. Paul Rousteau, and Peter Schroedl for
702 reviewing data products; Dr. Roland Hatzenpichler for reviewing an earlier version of the
703 manuscript; Brewster Kingham and Mark Shaw at the University of Delaware DNA Sequencing
704 and Genotyping Center for sequencing services and troubleshooting; and Thomas Symancyk and
705 Zachary Jones for logistical and shipment support. This work was performed under the auspices
706 U.S. Department of Energy Grant #DE-SC0022193 and NASA Exobiology Grant
707 #80NSSC23K0224.

708 **References**

709 1. Kuru E, Hughes HV, Brown PJ, Hall E, Tekkam S, Cava F, de Pedro MA, Brun YV,
710 VanNieuwenhze MS. 2012. In situ probing of newly synthesized peptidoglycan in live bacteria
711 with fluorescent D-amino acids. Angewandte Chemie 124:12687–12691.

712 2. Doud DF, Bowers RM, Schulz F, De Raad M, Deng K, Tarver A, Glasgow E, Vander
713 Meulen K, Fox B, Deutsch S. 2020. Function-driven single-cell genomics uncovers cellulose-
714 degrading bacteria from the rare biosphere. The ISME journal 14:659–675.

715 3. Lawrence AD, Nemoto-Smith E, Deery E, Baker JA, Schroeder S, Brown DG, Tullet JM,
716 Howard MJ, Brown IR, Smith AG. 2018. Construction of fluorescent analogs to follow the
717 uptake and distribution of cobalamin (vitamin B12) in bacteria, worms, and plants. Cell chemical
718 biology 25:941–951.

719 4. Hatzenpichler R, Scheller S, Tavormina PL, Babin BM, Tirrell DA, Orphan VJ. 2014. In
720 situ visualization of newly synthesized proteins in environmental microbes using amino acid
721 tagging and click chemistry. Environ Microbiol 16:2568–2590.

722 5. Hatzenpichler R, Connon SA, Goudeau D, Malmstrom RR, Woyke T, Orphan VJ. 2016.
723 Visualizing in situ translational activity for identifying and sorting slow-growing archaeal−
724 bacterial consortia. Proceedings of the National Academy of Sciences 113:E4069–E4078.

725 6. Steward KF, Eilers B, Tripet B, Fuchs A, Dorle M, Rawle R, Soriano B,
726 Balasubramanian N, Copié V, Bothner B. 2020. Metabolic implications of using BioOrthogonal
727 Non-Canonical Amino Acid Tagging (BONCAT) for tracking protein synthesis. Frontiers in
728 microbiology 11:197.

729 7. Best MD. 2009. Click chemistry and bioorthogonal reactions: unprecedented selectivity
730 in the labeling of biological molecules. Biochemistry 48:6571–6584.

731 8. Sletten EM, Bertozzi CR. 2009. Bioorthogonal chemistry: fishing for selectivity in a sea
732 of functionality. Angewandte Chemie International Edition 48:6974–6998.

733 9. Ignacio BJ, Dijkstra J, Mora N, Slot EF, van Weijsten MJ, Storkebaum E, Vermeulen M,
734 Bonger KM. 2023. THRONCAT: metabolic labeling of newly synthesized proteins using a
735 bioorthogonal threonine analog. Nature communications 14:3367.

736 10. Reichart NJ, Jay ZJ, Krukenberg V, Parker AE, Spietz RL, Hatzenpichler R. 2020.
737 Activity-based cell sorting reveals responses of uncultured archaea and bacteria to substrate
738 amendment. The ISME journal 14:2851–2861.

739 11. Frates ES, Spietz RL, Silverstein MR, Girguis P, Hatzenpichler R, Marlow JJ. 2023.
740 Natural and anthropogenic carbon input affect microbial activity in salt marsh sediment.
741 Frontiers in Microbiology 14:1235906.

742 12. Couradeau E, Sasse J, Goudeau D, Nath N, Hazen TC, Bowen BP, Chakraborty R,
743 Malmstrom RR, Northen TR. 2019. Probing the active fraction of soil microbiomes using
744 BONCAT-FACS. Nature communications 10:2770.

745 13. Trexler RV, Van Goethem MW, Goudeau D, Nath N, Malmstrom RR, Northen TR,
746 Couradeau E. 2023. BONCAT-FACS-Seq reveals the active fraction of a biocrust community
747 undergoing a wet-up event. Frontiers in Microbiology 14:1176751.

748 14. Hatzenpichler R, Orphan VJ. 2015. Detection of protein-synthesizing microorganisms in
749 the environment via bioorthogonal non-canonical amino acid tagging (BONCAT). Hydrocarbon
750 and Lipid Microbiology Protocols 145.

751 15. Marlow JJ, Colocci I, Jungbluth SP, Weber NM, Gartman A, Kallmeyer J. 2020.
752 Mapping metabolic activity at single cell resolution in intact volcanic fumarole sediment. FEMS
753 microbiology letters 367:fnaa031.

754 16. Landor LA, Bratbak G, Larsen A, Tjendra J, Våge S. 2023. Differential toxicity of
755 bioorthogonal non-canonical amino acids (BONCAT) in Escherichia coli. Journal of
756 Microbiological Methods 206:106679.

757 17. Hatzenpichler R, Krukenberg V, Spietz RL, Jay ZJ. 2020. Next-generation physiology
758 approaches to study microbiome function at single cell level. Nature Reviews Microbiology
759 18:241–256.

760 18. Ackermann M. 2015. A functional perspective on phenotypic heterogeneity in
761 microorganisms. Nature Reviews Microbiology 13:497–508.

762 19. Lidstrom ME, Konopka MC. 2010. The role of physiological heterogeneity in microbial
763 population behavior. Nature chemical biology 6:705–712.

764 20. Larsen S, Nielsen LP, Schramm A. 2015. Cable bacteria associated with long-distance
765 electron transport in N ew E ngland salt marsh sediment. Environmental microbiology reports
766 7:175–179.

767 21. Wilbanks EG, Jaekel U, Salman V, Humphrey PT, Eisen JA, Facciotti MT, Buckley DH,
768 Zinder SH, Druschel GK, Fike DA. 2014. Microscale sulfur cycling in the phototrophic pink
769 berry consortia of the Sippewissett Salt Marsh. Environmental microbiology 16:3398–3415.

770 22. Marlow J, Spietz R, Kim K, Ellisman M, Girguis P, Hatzenpichler R. 2021. Spatially
771 resolved correlative microscopy and microbial identification reveal dynamic depth-and mineral-
772 dependent anabolic activity in salt marsh sediment. Environmental Microbiology 23:4756–4777.

773 23. Wilbanks EG, Salman-Carvalho V, Jaekel U, Humphrey PT, Eisen JA, Buckley DH,
774 Zinder SH. 2017. The Green Berry Consortia of the Sippewissett Salt Marsh: millimeter-sized
775 aggregates of diazotrophic unicellular cyanobacteria. Frontiers in microbiology 8:1623.

776 24. Kiick KL, Saxon E, Tirrell DA, Bertozzi CR. 2002. Incorporation of azides into
777 recombinant proteins for chemoselective modification by the Staudinger ligation. Proceedings of
778 the National academy of Sciences 99:19–24.

779 25. Anthony C. 1991. Assimilation of carbon by methylotrophs. Biology of methylotrophs
780 18:79–109.

781 26. Knief C, Ramette A, Frances L, Alonso-Blanco C, Vorholt JA. 2010. Site and plant
782 species are important determinants of the Methylobacterium community composition in the plant
783 phyllosphere. The ISME journal 4:719–728.

784 27. Whiting G, Gandy EL, Yoch DC. 1986. Tight coupling of root-associated nitrogen
785 fixation and plant photosynthesis in the salt marsh grass Spartina alterniflora and carbon dioxide
786 enhancement of nitrogenase activity. Applied and environmental microbiology 52:108–113.

787 28. Van Gemerden H. 1968. On the ATP generation by Chromatium in darkness. Archiv für
788 Mikrobiologie 64:118–124.

789 29. Rothermich MM, Guerrero R, Lenz RW, Goodwin S. 2000. Characterization, seasonal
790 occurrence, and diel fluctuation of poly (hydroxyalkanoate) in photosynthetic microbial mats.
791 Applied and Environmental Microbiology 66:4279–4291.

792 30. Baltar F, Martínez-Pérez C, Amano C, Vial M, Robaina-Estévez S, Reinthaler T, Herndl
793 GJ, Zhao Z, Logares R, Morales SE. 2023. A ubiquitous gammaproteobacterial clade dominates
794 expression of sulfur oxidation genes across the mesopelagic ocean. Nature Microbiology
795 8:1137–1148.

796 31. Salman V, Yang T, Berben T, Klein F, Angert E, Teske A. 2015. Calcite-accumulating
797 large sulfur bacteria of the genus Achromatium in Sippewissett Salt Marsh. The ISME journal
798 9:2503–2514.

799 32. George Matlalcuatzi ED, Bakkum T, Thomas PS, Hacker S, Florea BI, Vriesendorp B,
800 Rozen DE, van Kasteren SI. 2025. Using BONCAT to dissect the proteome of S. aureus
801 persisters. Msphere 10:e00431-25.

802 33. Han S, Luo X, Hao X, Ouyang Y, Zeng L, Wang L, Wen S, Wang B, Van Nostrand JD,
803 Chen W. 2021. Microscale heterogeneity of the soil nitrogen cycling microbial functional
804 structure and potential metabolism. Environmental Microbiology 23:1199–1209.

805 34. Cordero OX, Datta MS. 2016. Microbial interactions and community assembly at
806 microscales. Current opinion in microbiology 31:227–234.

807 35. Schindelin J, Arganda-Carreras I, Frise E, Kaynig V, Longair M, Pietzsch T, Preibisch S,
808 Rueden C, Saalfeld S, Schmid B. 2012. Fiji: an open-source platform for biological-image
809 analysis. Nature methods 9:676–682.

810 36. Lin M, Comings D, Alfi O. 1977. Optical studies of the interaction of 4′-6-diamidino-2-
811 phenylindole with DNA and metaphase chromosomes. Chromosoma 60:15–25.

812 37. Larsen TA, Goodsell DS, Cascio D, Grzeskowiak K, Dickerson RE. 1989. The structure
813 of DAPI bound to DNA. Journal of Biomolecular Structure and Dynamics 7:477–491.

814 38. Ross J, Boon P, Sharma R, Beckett R. 1996. Variations in the fluorescence intensity of
815 intact DAPI-stained bacteria and their implications for rapid bacterial quantification. Letters in
816 applied microbiology 22:283–287.

817 39. Walberg M, Gaustad P, Steen HB. 1999. Uptake kinetics of nucleic acid targeting dyes
818 inS. aureus, E. faecalis andB. cereus: a flow cytometric study. Journal of microbiological
819 methods 35:167–176.

820 40. Huber H, Huber G, Stetter KO. 1985. A modified DAPI fluorescence staining procedure
821 suitable für the visualization of lithotrophic bacteria. Systematic and applied microbiology
822 6:105–106.

823 41. Bock N, Subramaniam A, Juhl AR, Montoya J, Duhamel S. 2022. Quantifying per-cell
824 chlorophyll a in natural picophytoplankton populations using fluorescence-activated cell sorting.
825 Frontiers in Marine Science 9:850646.

826 42. Doyle JJ, Doyle JL. 1987. A rapid DNA isolation procedure for small quantities of fresh
827 leaf tissue. Phytochemical bulletin.

828 43. Natarajan VP, Zhang X, Morono Y, Inagaki F, Wang F. 2016. A modified SDS-based
829 DNA extraction method for high quality environmental DNA from seafloor environments.
830 Frontiers in microbiology 7:986.

831 44. Thompson LR, Sanders JG, McDonald D, Amir A, Ladau J, Locey KJ, Prill RJ, Tripathi
832 A, Gibbons SM, Ackermann G. 2017. A communal catalogue reveals Earth's multiscale
833 microbial diversity. Nature.

834 45. Parada AE, Needham DM, Fuhrman JA. 2016. Every base matters: assessing small
835 subunit rRNA primers for marine microbiomes with mock communities, time series and global
836 field samples. Environ Microbiol 18:1403–1414.

837 46. Apprill A, McNally S, Parsons R, Weber L. 2015. Minor revision to V4 region SSU
838 rRNA 806R gene primer greatly increases detection of SAR11 bacterioplankton. Aquatic
839 Microbial Ecology 75:129–137.

840 47. Bolyen E, Rideout JR, Dillon MR, Bokulich NA, Abnet CC, Al-Ghalith GA, Alexander
841 H, Alm EJ, Arumugam M, Asnicar F. 2019. Reproducible, interactive, scalable and extensible
842 microbiome data science using QIIME 2. Nature biotechnology 37:852–857.

843 48. Sweetman AK, Smith AJ, de Jonge DS, Hahn T, Schroedl P, Silverstein M, Andrade C,
844 Edwards RL, Lough AJ, Woulds C. 2024. Evidence of dark oxygen production at the abyssal
845 seafloor. Nature Geoscience 17:737–739.

846 49. Silverstein MR, Bhatnagar JM, Segrè D. 2024. Metabolic complexity drives divergence
847 in microbial communities. Nature Ecology & Evolution 8:1493–1504.

848 50. Martin M. 2011. Cutadapt removes adapter sequences from high-throughput sequencing
849 reads. EMBnet journal 17:10–12.

850 51. Callahan BJ, McMurdie PJ, Rosen MJ, Han AW, Johnson AJA, Holmes SP. 2016.
851 DADA2: high-resolution sample inference from Illumina amplicon data. Nature methods
852 13:581–583.

853 52. Yilmaz P, Parfrey LW, Yarza P, Gerken J, Pruesse E, Quast C, Schweer T, Peplies J,
854 Ludwig W, Glöckner FO. 2014. The SILVA and "all-species living tree project (LTP)"
855 taxonomic frameworks. Nucleic acids research 42:D643–D648.

856 53. Rognes T, Flouri T, Nichols B, Quince C, Mahé F. 2016. VSEARCH: a versatile open
857 source tool for metagenomics. PeerJ 4:e2584.

858 54. McMurdle P, Holmes S. 2013. Handling and analysis of high-throughput microbiome
859 census data. Bioconductor.

860

861

862

863

864

865

866

867

868

869

870

871

872

873 Fig. S1: Representative fields of view from mono-BONCAT experiments with *E. coli* cultures,

874 evaluating fluorescence signals derived from a range of HPG and Azide-Cy3 concentrations. All

875 scale bars are 10 µm.

876

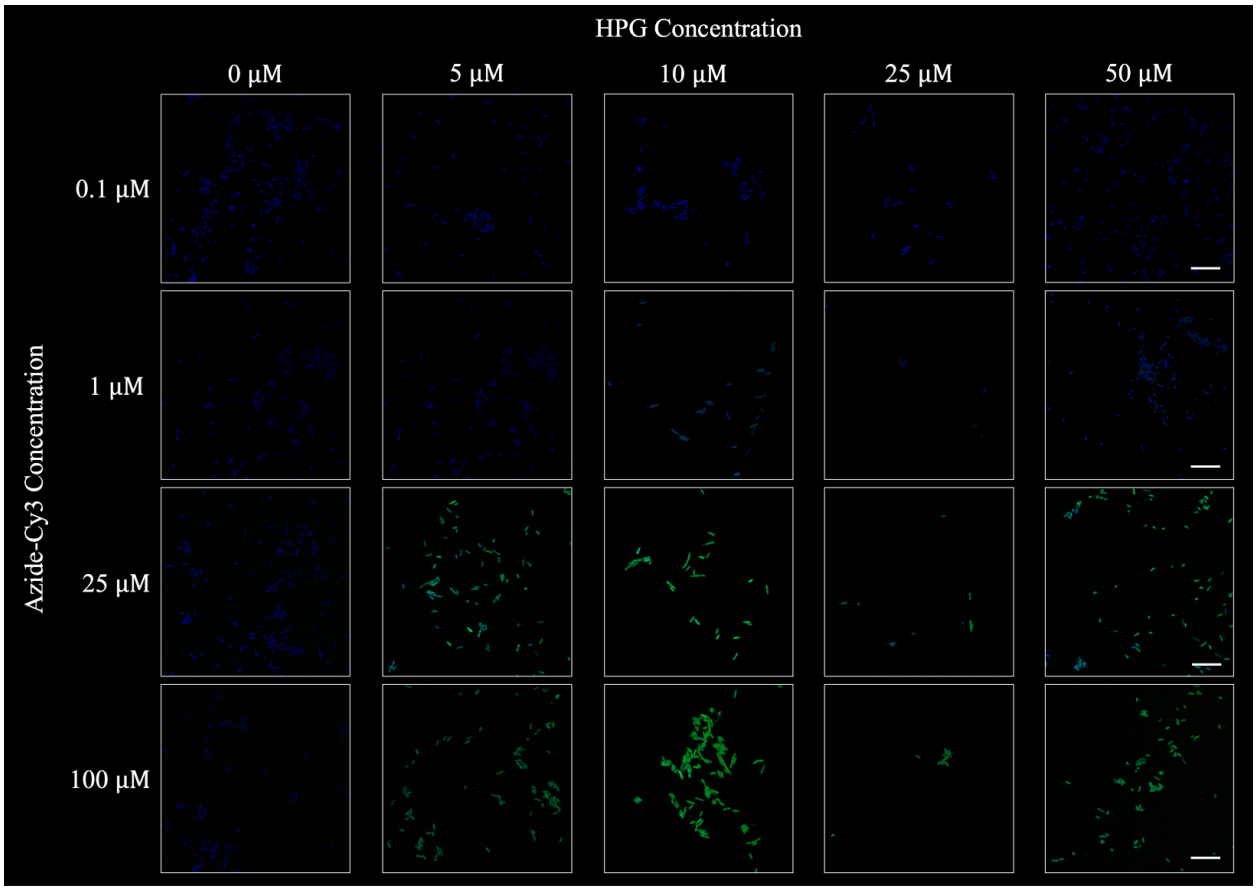

877

878

879

880

881

882

883

884

885 Fig. S2: Representative fields of view from mono-BONCAT experiments with *E. coli* cultures,

886 evaluating fluorescence signals derived from a range of AHA and DBCO-Cy5 concentrations.

887 All scale bars are 10 µm.

888

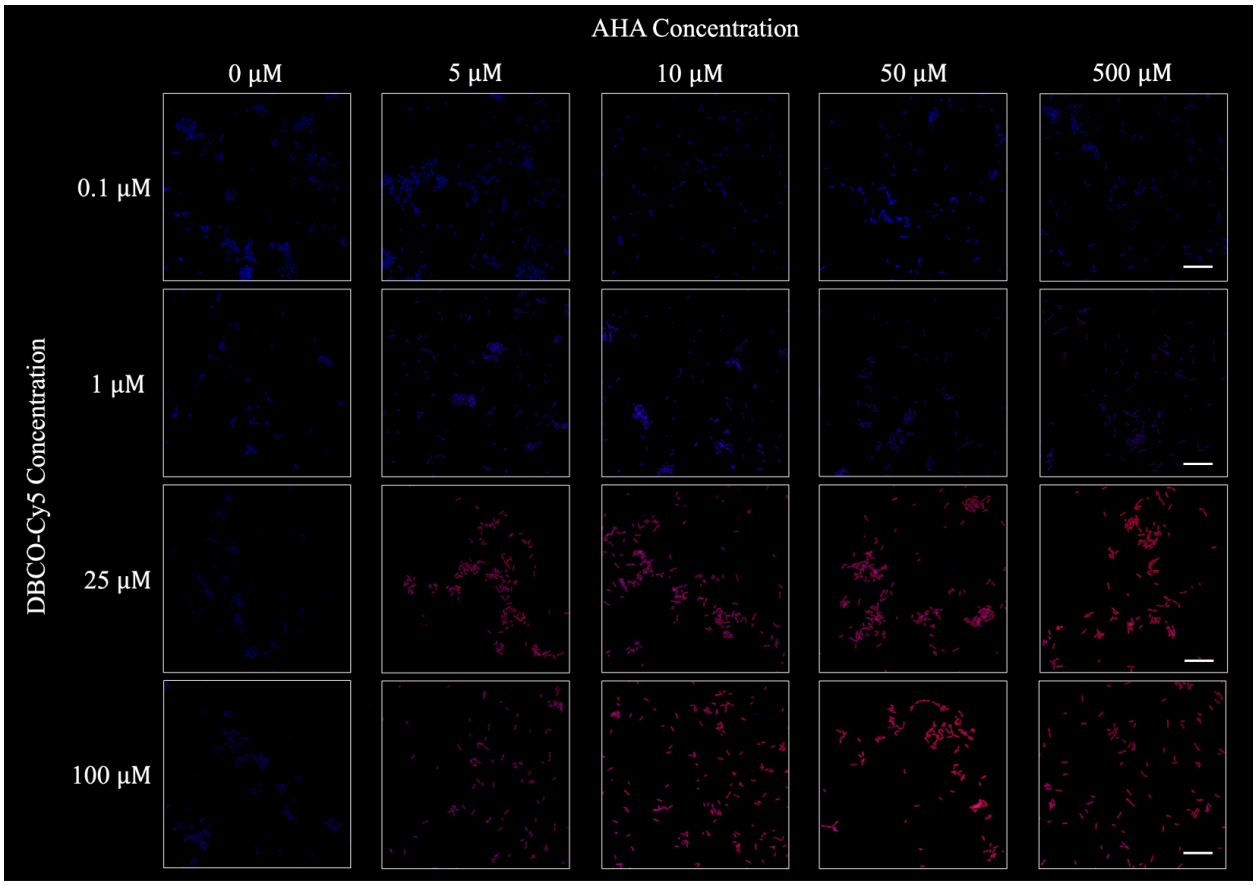

889

890

891

892

893

894

895

896

Fig. S3: Boxplots of mean fluorescence intensity values of cells in mono-BONCAT experiments with *E. coli* cultures. A range of ncAA and dye concentrations were tested to determine parameters for subsequent dual-BONCAT experiments. Imaging parameters were consistent across all different conditions.

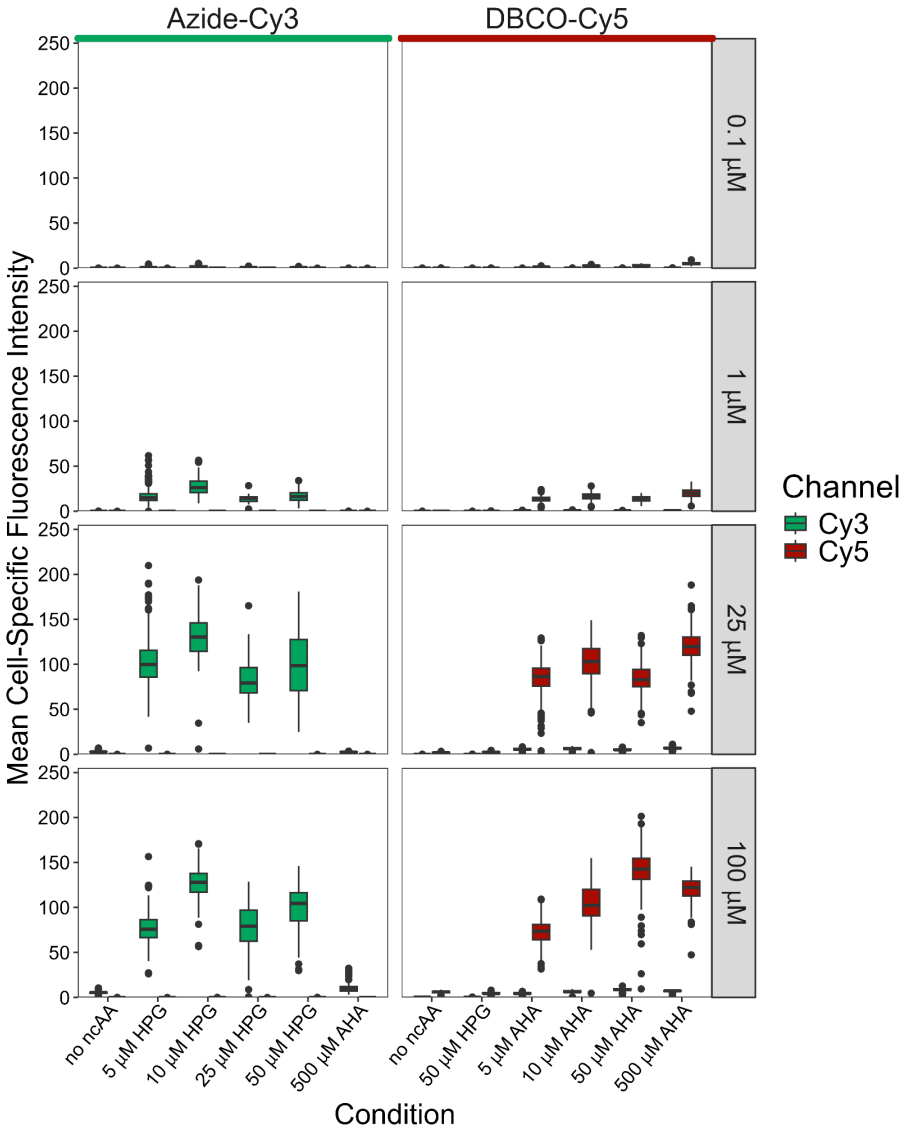

Fig. S4: Representative fields of view from dual-BONCAT experiments with *E. coli* cultures, evaluating the order of ncAA addition and performing the HPG-Azide reaction first followed by the AHA-DBCO. All scale bars indicate 10 µm.

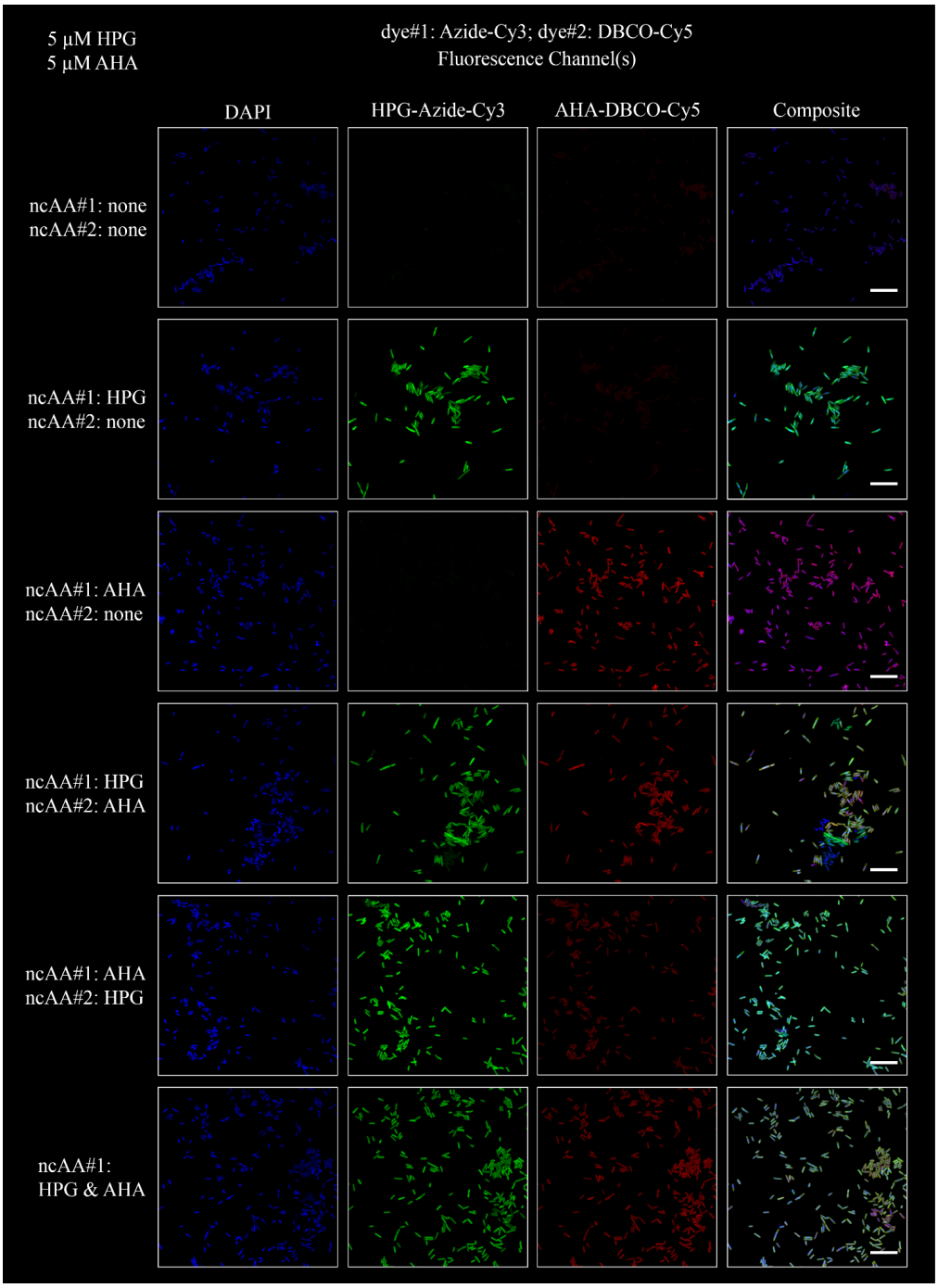

Fig. S5: Representative fields of view from dual-BONCAT experiments with *E. coli* cultures, evaluating the order of ncAA addition and performing the AHA-DBCO reaction first followed by the HPG-Azide reaction. All scale bars indicate 10 µm.

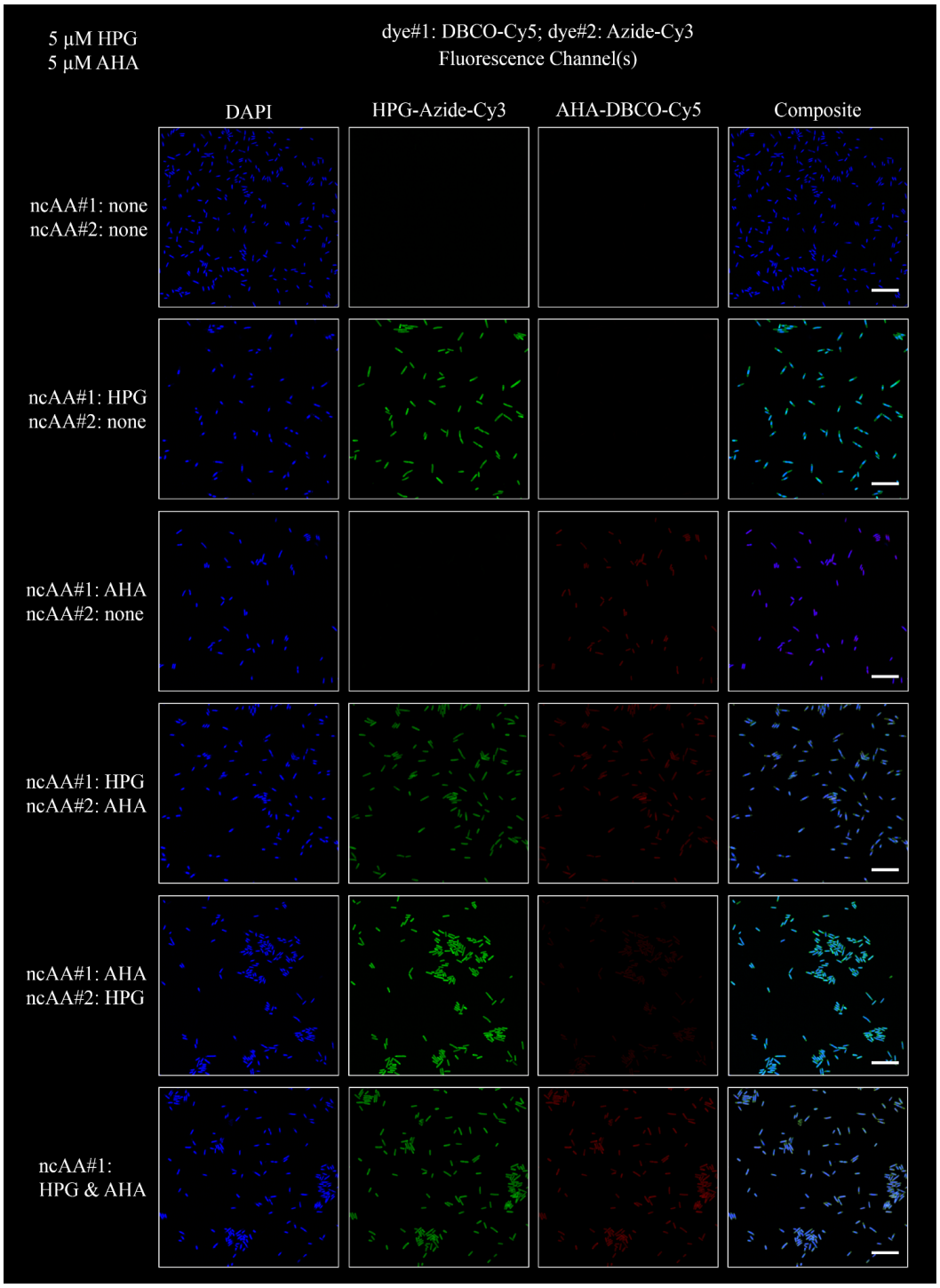

913 Fig. 1: Boxplots of mean fluorescence intensity values of cells in dual-BONCAT experiments
914 with *E. coli* cultures. Tests varying the sequence of ncAA addition (see column labels along x-
915 axis) were performed, with the Azide-Cy3 click reaction conducted first (left panel) and with the
916 DBCO-Cy5 click reaction conducted first (middle panel). The procedural control in which *E.*
917 *coli* cells were mono-labeled and mono-stained is shown in the right panel.

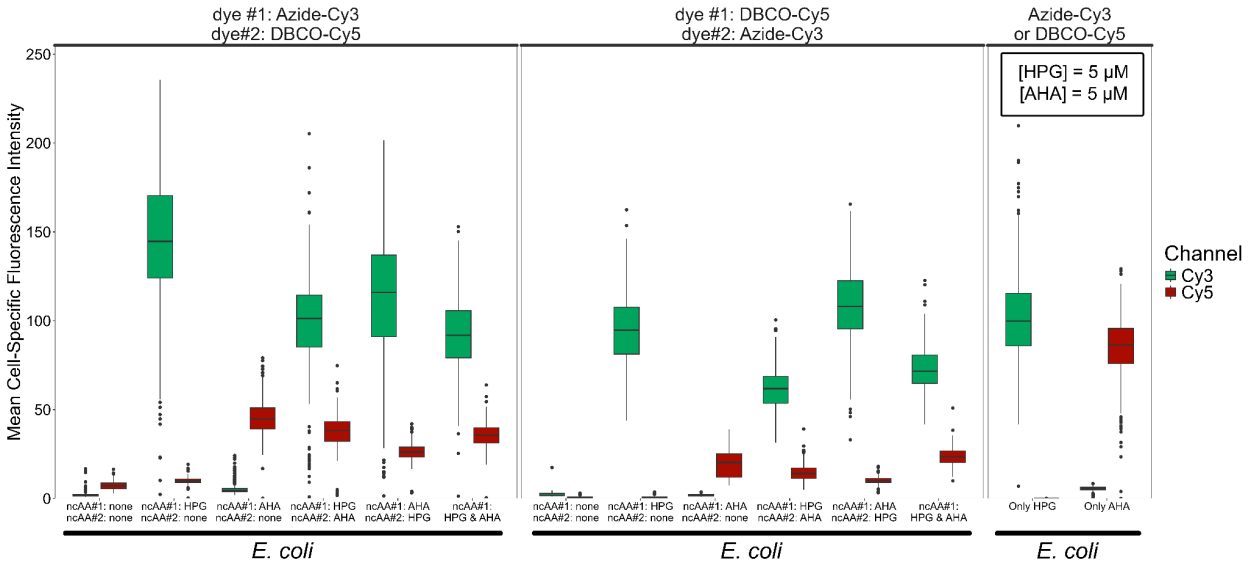

918

919

920

921

922

923

924

925

926 Fig. S6: Fluorescence microscopy field of view of a dual-BONCAT experiment with *E. coli*

927 cells. Both ncAAs were added at the start of the experiment, and, following fixation, the Azide-

928 Cy3 click reaction was performed first. Scale bar indicates 5 µm.

929 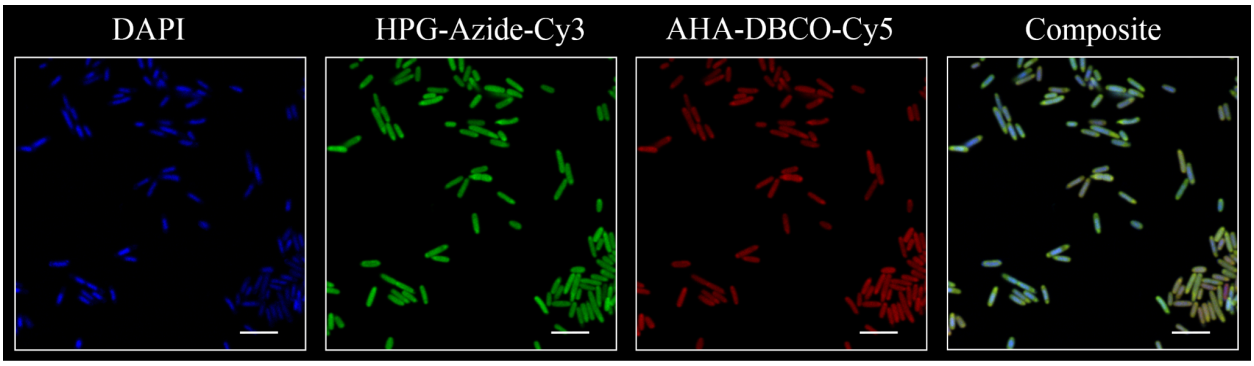

930

931

932

933

934

935

936

937

938

939

Fig. S7: Ratio of the Cy3 to Cy5 fluorescent intensities for the experiment in which HPG and AHA were added at T_1 in the field of view chosen for Fig. S6 (left), and the experiment in which HPG was added at T_1 and AHA at T_2 in the field of view chosen for Fig. 2 (right). Cells whose mean intensities exceeded the maximum intensities in the "no ncAA" condition were considered labelled. The red-colored bar indicates the cell labeled with a red arrow in Fig. 2; the bar marked with a red asterisk indicates the two cells labeled with red arrows and asterisks in Fig. 2.

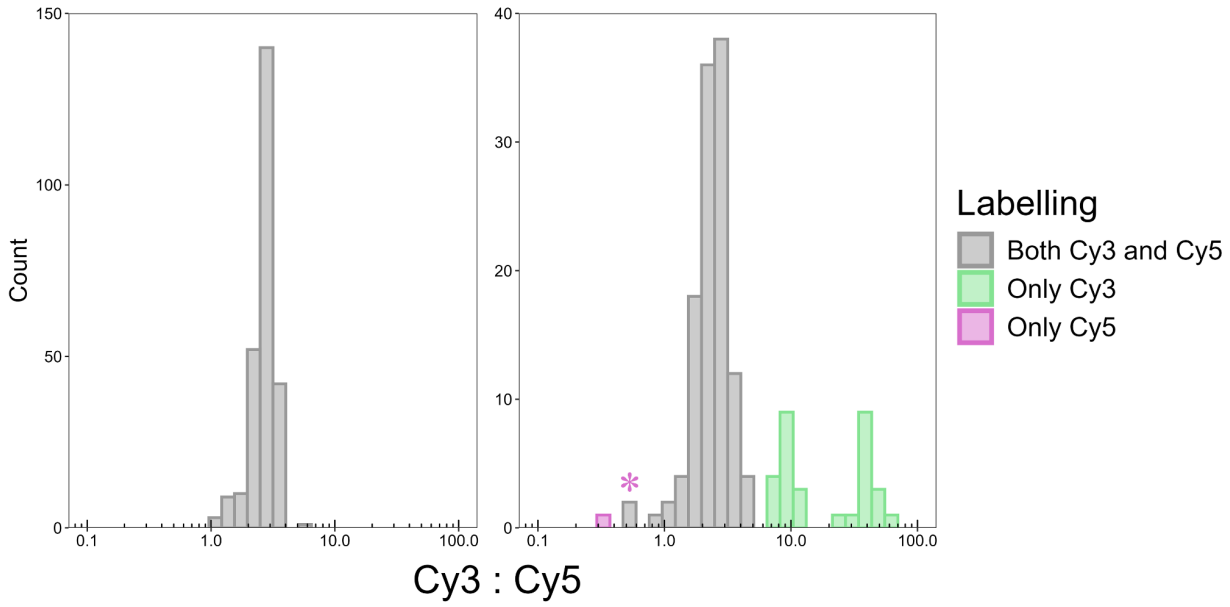

Fig. 2: Fluorescence microscopy field of view of a dual-BONCAT experiment with *E. coli* cells. HPG was added at the start of the experiment; AHA was added 8 hours later, and the experiment was stopped after 24 hours. The Azide-Cy3 click reaction was performed first. Arrows indicate select cells representative of the distinct subpopulations identifiable with dual-BONCAT. Blue arrows: cells that were not labeled with either ncAA. White arrows: cells that incorporated both ncAAs. Green arrows: cells that only incorporated HPG. Magenta arrows: cells that only incorporated AHA. Magenta arrows with asterisks indicate cells with very low Cy3:Cy5 ratios (see Fig. S7) that dominantly incorporated AHA, but whose Cy3 intensities were slightly above the threshold value set for our binary "labelled" designation. Scale bar indicates 5 µm.

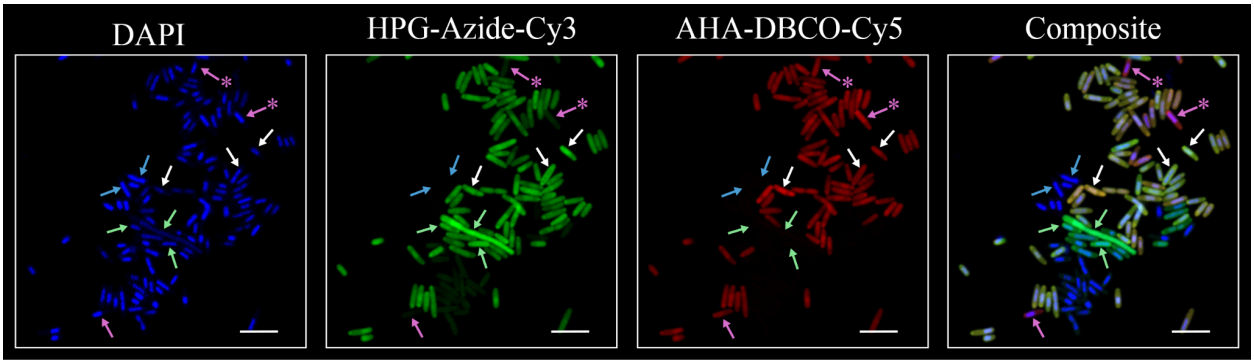

970 Fig. 3: Boxplots of mean fluorescence intensity values of cells in dual-BONCAT experiments
971 with extracted salt marsh sediment cells. Tests varying the sequence of ncAA addition (see
972 column labels along x-axis) were performed, with the Azide-Cy3 click reaction conducted first
973 (left panel) and with the DBCO-Cy5 click reaction conducted first (middle panel). A) Data from
974 the 50 µM HPG & 50 µM AHA condition; B) data from the 50 µM HPG & 500 µM AHA
975 condition.

976 A)

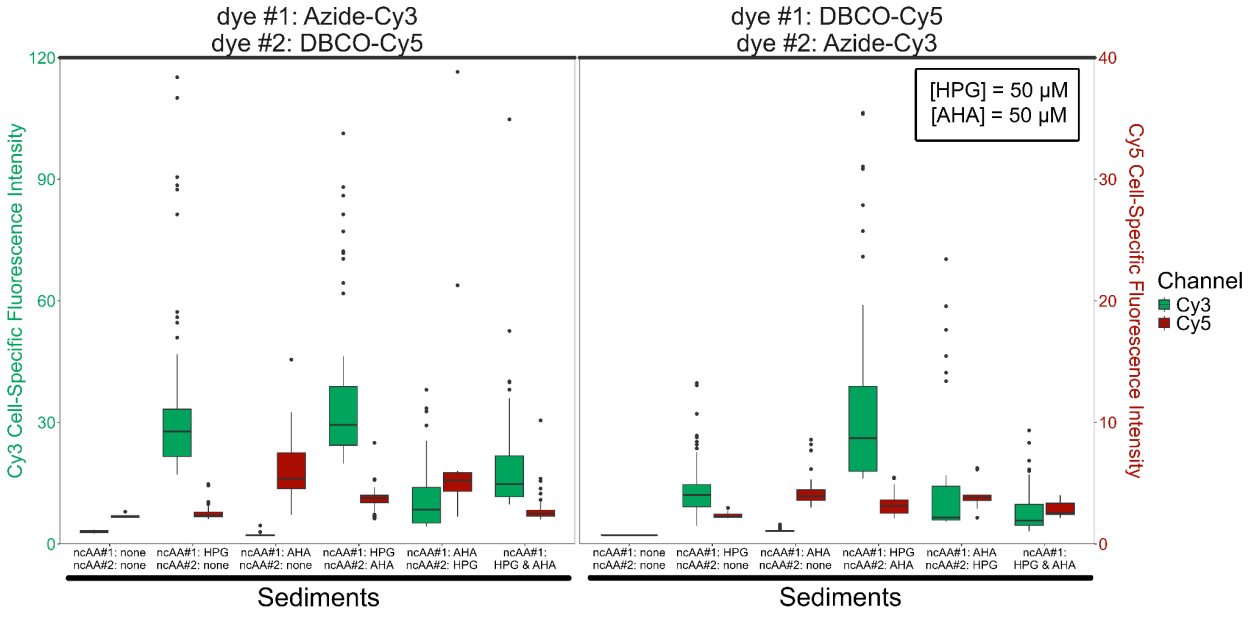

977

978 B)

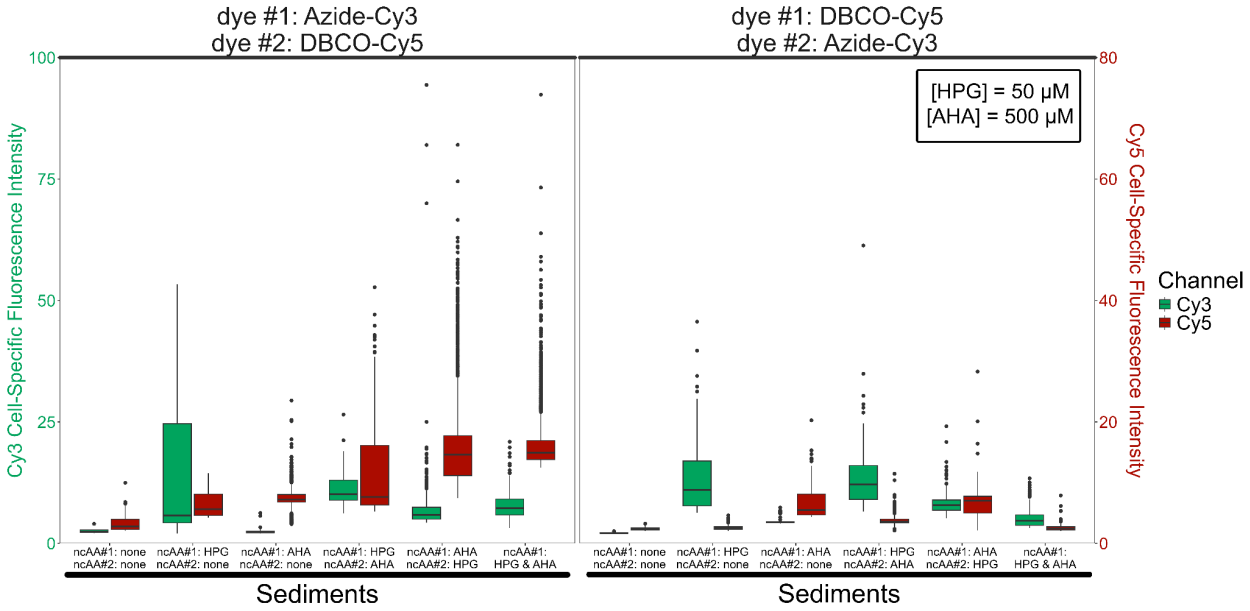
dye #1: Azide-Cy3
dye #2: DBCO-Cy5
dye #1: DBCO-Cy5
dye #2: Azide-Cy3
[HPG] = 50 μM
[AHA] = 500 μM
Cy3 Cell-Specific Fluorescence Intensity
Cy5 Cell-Specific Fluorescence Intensity
Channel
Cy3
Cy5
ncAA#1: none
ncAA#2: none
ncAA#1: HPG
ncAA#2: none
ncAA#1: AHA
ncAA#2: none
ncAA#1: HPG
ncAA#2: AHA
ncAA#1: AHA
ncAA#2: HPG
ncAA#1:
HPG & AHA
Sediments
Sediments

Fig. S8: Representative fields of view from dual-BONCAT experiments with extracted cells from salt marsh sediments, evaluating the order of ncAA addition and performing the HPG-azide reaction first followed by the AHA-DBCO. All scale bars indicate 10 µm.

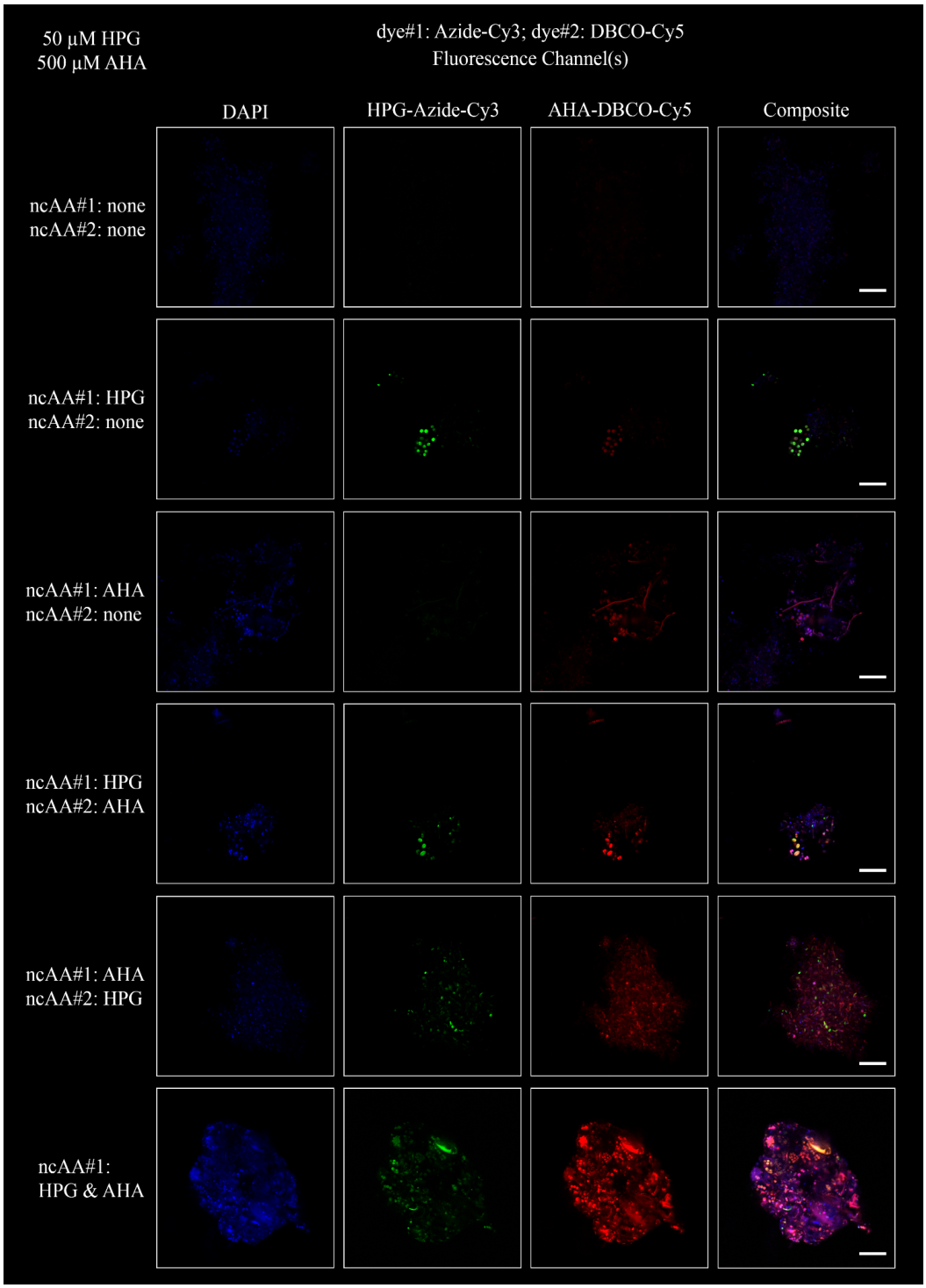

Fig. S9: Representative fields of view from dual-BONCAT experiments with extracted cells from salt marsh sediments, evaluating the order of ncAA addition and performing the DBCO-Cy5 reaction first followed by the HPG-azide. All scale bars indicate 10 µm.

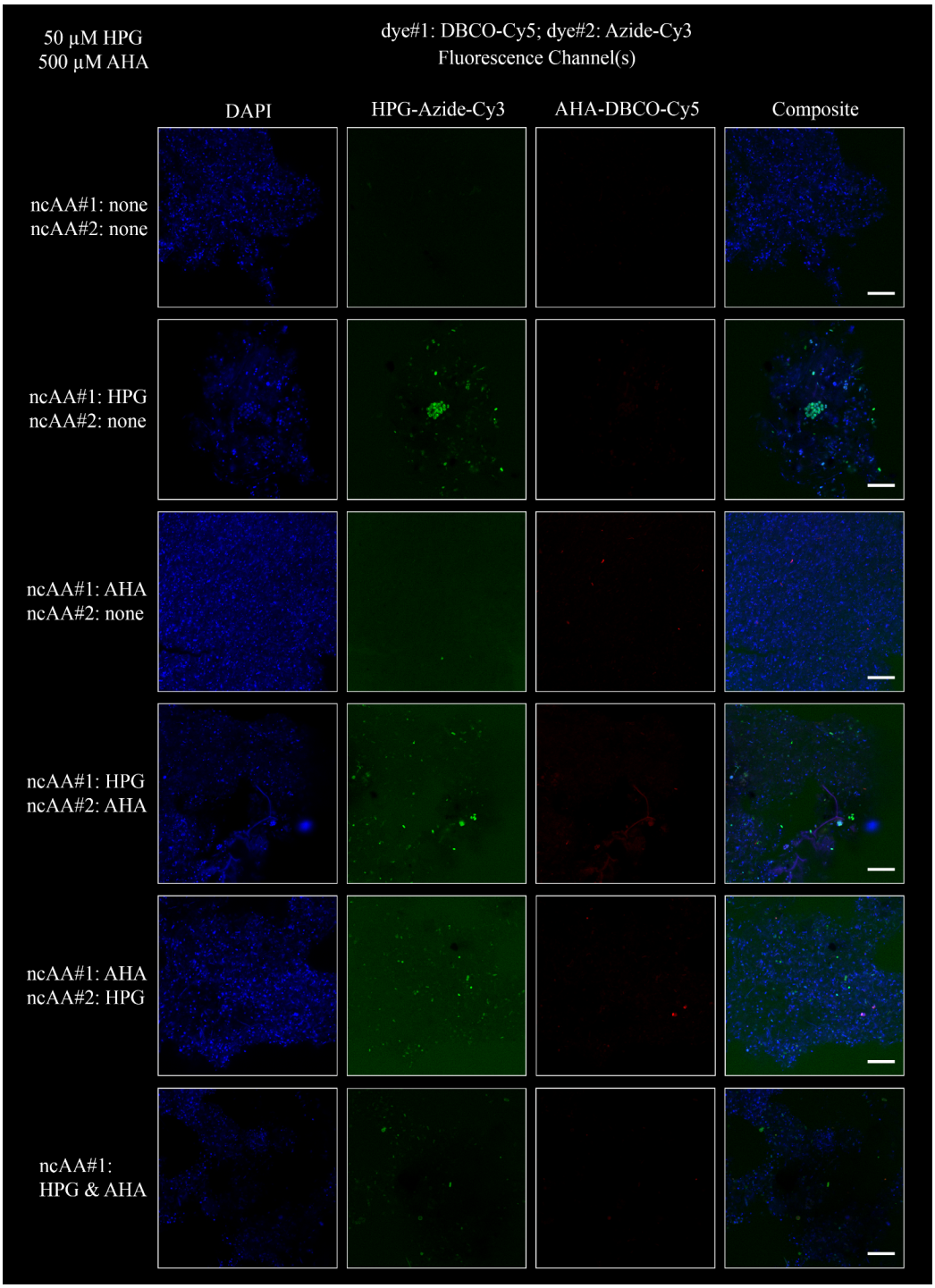

Fig. S10: Boxplots of mean fluorescence intensity values of cells in dual-BONCAT experiments with extracted salt marsh sediment cells. Tests varying the sequence of ncAA addition (see column labels along x-axis) were performed, with the Azide-Cy3 click reaction conducted first (left panel) and with the DBCO-Cy5 click reaction conducted first (middle panel). Data from the 5 µM HPG & 5 µM AHA condition.

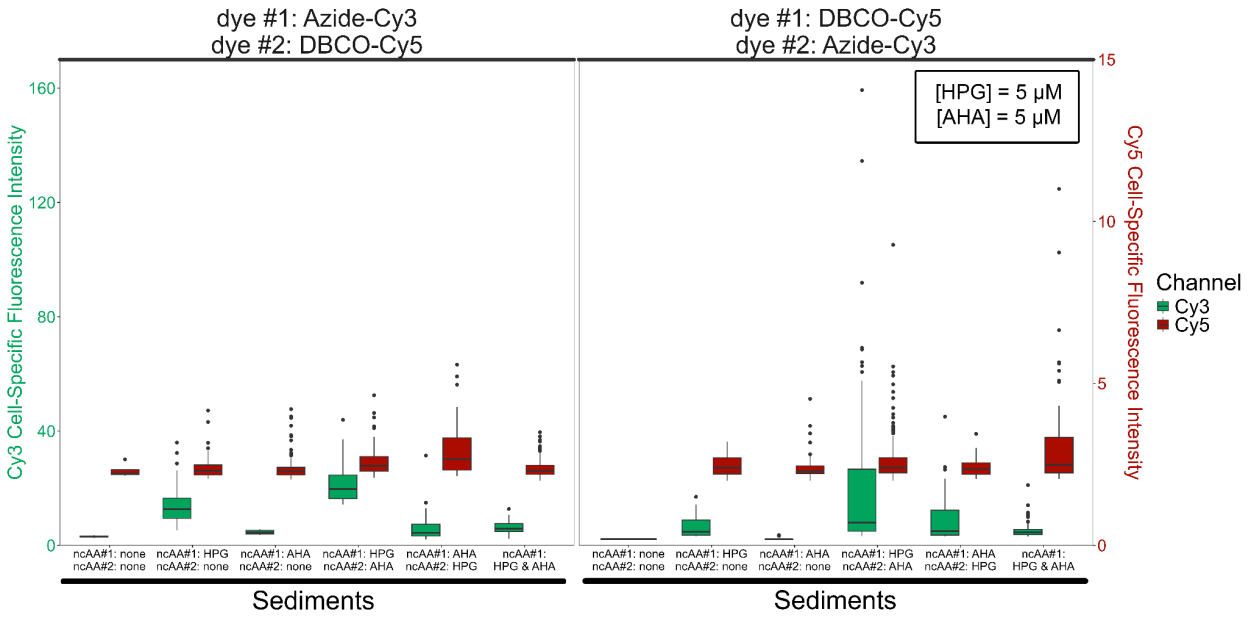

1009 Fig. S11: Fluorescence microscopy field of view of a dual-BONCAT experiment with extracted

1010 salt marsh sediment cells. Both ncAAs (50 µM HPG & 500 µM AHA) were added at the start of

1011 the experiment, which was stopped after a single, 24-hour day-night cycle. The Azide-Cy3 click

1012 reaction was performed first. Scale bar indicates 5 µm.

1013 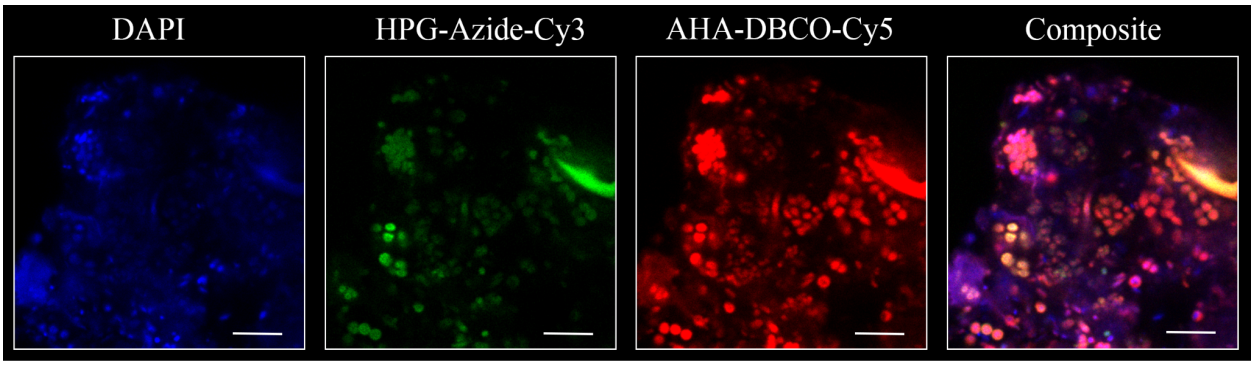

1014

1015

1016

1017

1018

1019

1020

1021

1022

1023 Fig. 4: Fluorescence microscopy field of view of a dual-BONCAT experiment with extracted salt
1024 marsh sediment cells. 50 µM HPG was added at the start of the experiment; 500 µM AHA was
1025 added 12 hours later, and the experiment was stopped after a single 24-hour day-night cycle. The
1026 Azide-Cy3 click reaction was performed first. Arrows indicate select cells representative of the
1027 distinct subpopulations identifiable with dual-BONCAT. Blue arrows: cells that were not labeled
1028 with either ncAA. White arrows: cells that incorporated both ncAAs. Green arrows: cells that
1029 only incorporated HPG. Magenta arrows: cells that only incorporated AHA. Scale bar indicates 5
1030 µm.

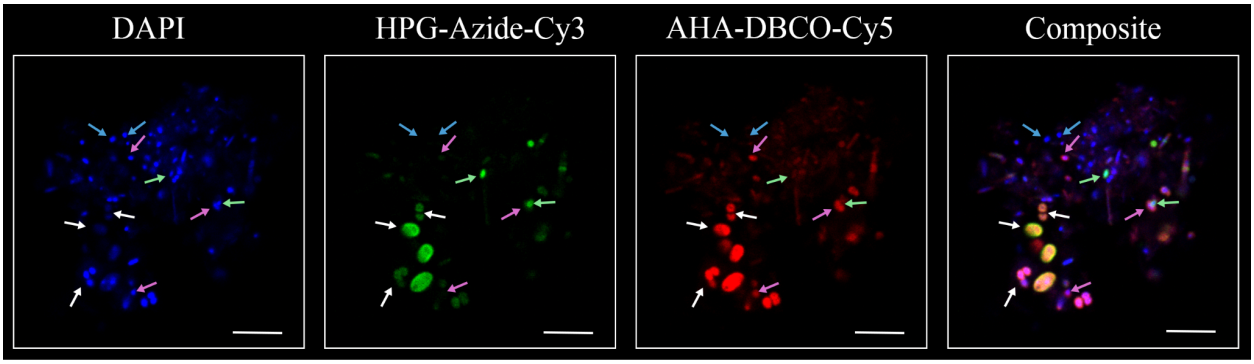

1031

1032

1033

1034

1035

1036

1037

1038

1039 Fig. S12: An interpretive scheme for dual-BONCAT experiments. For a generalized
1040 experimental timeline during which one ncAA is added at an initial time point (T_1) and a second
1041 ncAA is added at a subsequent time point (T_2), the three distinct subpopulations of labeled cells
1042 (e.g., those labeled with only ncAA#1, both ncAA#1&2, and only ncAA#2) can be interpreted as
1043 being anabolically active during distinct phases of the experiment. Further details are provided in
1044 the text.

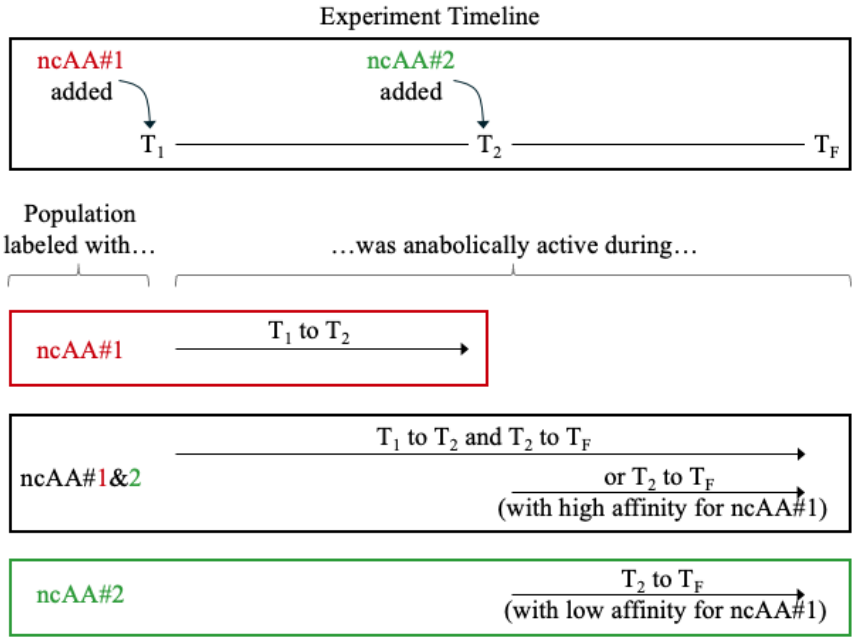

1045

1046

1047

1048

1049

1050

Fig. S13: Schematic representation of the subpopulations gating protocol. (1) Gate single cells subpopulation on a trigger pulse width versus forward scatter plot, (2) Gate Cy3 negative subpopulation by analyzing a ncAA-free sample with Cy3 and a Cy5 mono-labeled sample on the Cy3 plot [585/29 nm emission at 561 nm excitation versus forward scatter], (3) Gate Cy3 positive subpopulation by analyzing a ncAA-Cy3 sample on the Cy3 plot and the Cy3Cy5 plot [692/40 nm emission at 640 nm excitation versus 585/29 nm emission at 561 nm excitation], (4) Gate Cy5 negative subpopulation by analyzing a ncAA-free sample with Cy5 and a Cy3 mono-labeled sample on the Cy5 plot [692/40 nm emission at 640 nm excitation versus forward scatter], (5) Gate Cy5 positive subpopulation by analyzing a ncAA-Cy5 sample on the Cy5 plot and the Cy3Cy5 plot, (6) Gate Cy3&Cy5 double-negative subpopulation by analyzing a ncAA-free sample with Cy3 and Cy5 on the Cy3Cy5 plot, (7) Gate Cy3&Cy5 double-positive subpopulation by analyzing a ncAA-Cy3&Cy5 sample on the Cy3Cy5 plot.

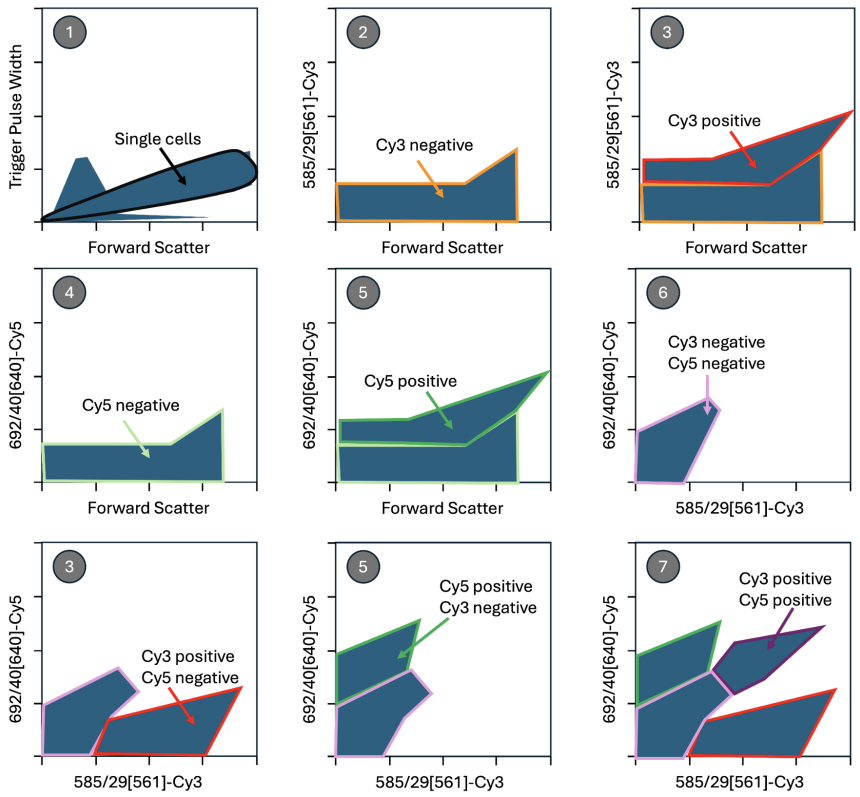

1064 Table S1: Number of sorted cells recovered from each gate of interest in this study.

Condition 1	
Subpopulation	*Number of Sorted Cells*
ncAA#1 active	718,584
ncAA#1&2 active	295,495
ncAA#2 active	Below Detection
Condition 2	
Subpopulation	*Number of Sorted Cells*
ncAA#1 active	21,424
ncAA#1&2 active	552,138
ncAA#2 active	321,110

1065

1066

1067

1068

1069

1070

1071

1072

1073

1074

1075

1076

1077 Fig. 5: Relative abundances of family-level taxonomic groupings derived from dual-BONCAT-
1078 FACS-16S analyses of LSSM sediments. Each row corresponds to a family that comprised at
1079 least 1% of the overall relative abundance in at least one of the five sorted and sequenced
1080 fractions. Each column and color corresponds to a given ncAA condition: yellow indicates cells
1081 that incorporated only ncAA#1 (regardless of which ncAA was added first), red indicates cells
1082 that incorporated both ncAAs (regardless of which was added first), and blue indicates cells that
1083 incorporated only ncAA#2 (when HPG was added second; the other condition did not result in
1084 sufficient cells for sequencing). The size of each circle indicates the mean relative abundance for
1085 a given family and ncAA condition; the faint "halo" around each data point conveys the standard
1086 deviation when two communities were sequenced for a given condition. See Table S2 for the
1087 data used to generate this figure.

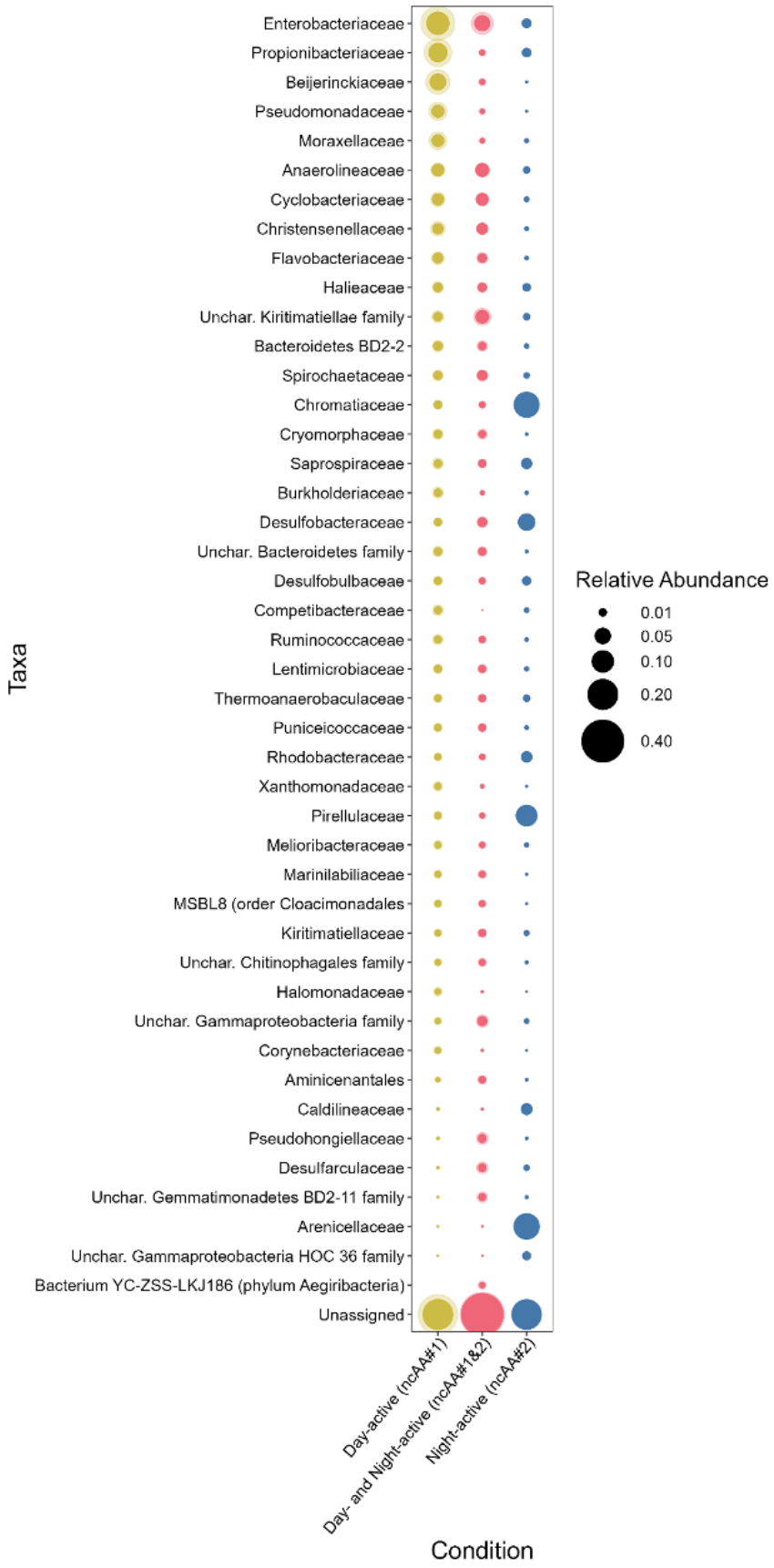
Taxa
Enterobacteriaceae
Propionibacteriaceae
Beijerinckiaceae
Pseudomonadaceae
Moraxellaceae
Anaerolineaceae
Cyclobacteriaceae
Christensenellaceae
Flavobacteriaceae
Halieaceae
Unchar. Kiritimatiellae family
Bacteroidetes BD2-2
Spirochaetaceae
Chromatiaceae
Cryomorphaceae
Saprospiraceae
Burkholderiaceae
Desulfobacteraceae
Unchar. Bacteroidetes family
Desulfobulbaceae
Competibacteraceae
Ruminococcaceae
Lentimicrobiaceae
Thermoanaerobaculaceae
Puniceicoccaceae
Rhodobacteraceae
Xanthomonadaceae
Pirellulaceae
Melioribacteraceae
Marinilabiliaceae
MSBL8 (order Cloacimonadales
Kiritimatiellaceae
Unchar. Chitinophagales family
Halomonadaceae
Unchar. Gammaproteobacteria family
Corynebacteriaceae
Aminicenantales
Caldilineaceae
Pseudohongiellaceae
Desulfarculaceae
Unchar. Gemmatimonadetes BD2-11 family
Arenicellaceae
Unchar. Gammaproteobacteria HOC 36 family
Bacterium YC-ZSS-LKJ186 (phylum Aegiribacteria)
Unassigned
Day-active (ncAA#1)
Day- and Night-active (ncAA#1&2)
Night-active (ncAA#2)
Condition
Relative Abundance
0.01
0.05
0.10
0.20
0.40

1088

1089 Table S2: Taxonomic identity and relative abundance of ASVs grouped at the family level for
1090 the seven communities sequenced in this study. Only family-level groupings that accounted for
1091 >1% of the relative abundance of at least one sequenced community are shown.

1092 *See Excel File*

1093

1094

1095

1096

1097

1098

1099

1100

1101

1102

1103

1104

1105

1106 Table S3: Taxonomic identity and relative abundance of all ASVs for the seven communities

1107 sequenced in this study.

1108 *See Excel File*

1109

1110

1111

1112

1113

1114

1115

1116

1117

1118

1119

1120

1121

1122

1123 Table S4: Components of the two premixes needed for the Cu(I)-catalyzed HPG-azide reaction.

1124

Premix 1			**Premix 2**	
Component	*Volume*		*Component*	*Volume*
100 mM Na-ascorbate	20 µL		20 mM $CuSO_4$	2 µL
100 mM Aminoguanidine-HCl	20 µL		50 mM THPTA	4 µL
1x PBS	344 µL		1 mM azide dye	10 µL

1125

1126

1127

1128

1129

1130

1131

1132

1133

1134

1135

1136

1137

1138 Table S5: Imaging parameters for the culture and environmental samples used in this study.

For *E. coli* cultures - 63x objective lens and 2.5x zoom				
Dye	**Laser Excitation**	**Detector Emission Window**	**Laser Intensity**	**Detector Gain**
DAPI	405 nm	420-559 nm	7.0%	8.0%
Cy3	554 nm	571-704 nm	2.0%	2.5%
Cy5	649 nm	666-750 nm	1.5%	2.5%
For LSSM Sediments - 63x objective lens and 2.5x zoom				
Dye	**Laser Excitation**	**Detector Emission Window**	**Laser Intensity**	**Detector Gain**
DAPI	405 nm	420-559 nm	7.0%	2.5%
Cy3	554 nm	571-704 nm	2.0%	2.5%
Cy5	649 nm	666-750 nm	1.5%	2.5%

1139

1140

1141

1142

1143

1144

1145

1146

1147

1148

1149

1150 Table S6: FIJI Multi-Channel Cell Counter plugin settings for the culture and environmental

1151 samples used in this study.

For *E. coli* cultures		
Dye	**Color**	**Min/Max**
DAPI	Blue	[0,100]
Cy3	Green	[0,200]
Cy5	Red	[0,100]
Manually Adjusted?	Yes	
Transformed?	Yes	
For LSSM Sediments		
Dye	**Color**	**Min/Max**
DAPI	Blue	[0,60]
Cy3	Green	[0,30]
Cy5	Red	[0,40]
Manually Adjusted?	Yes	
Transformed?	Yes	

1152

1153

1154

1155

1156

1157

1158

1159

1160 Table S7: FIJI Multi-Channel RGB Stacker plugin settings for the culture and environmental

1161 samples used in this study.

For *E. coli* cultures		
Dye	**Threshold**	**Counter-stain**
DAPI	None	Yes
Cy3	None	No
Cy5	None	No
Measurements:	Area, Min & Max, Mean, Standard Deviation	
Counter-stain Threshold:	Moments	
Watershed/Tolerance?	No	
Particle Size:	0.1-2 μm^2	
Particle Circularity	0-1	
Transformed?	Yes	
For LSSM Sediments		
Dye	**Threshold**	**Counter-stain**
DAPI	None	No
Cy3	None	Yes
Cy5	None	Yes
Measurements:	Area, Min & Max, Mean, Standard Deviation	
Counter-stain Threshold:	Moments	
Watershed/Tolerance?	Yes/0.5	
Particle Size:	0.1-4 μm^2	
Particle Circularity	0.2-1	
Transformed?	Yes	

1162

1163

1164

1165

1166

1167 Table S8: Alpha diversity metrics for the seven sequenced communities analyzed in this study.

1168

Sample	# of ASVs	Chao	ACE	Shannon	Evenness
Condition 1 Day-Active (ncAA#1)	4212	4629.2	4588.3	6.74	0.81
Condition 2 Day-Active (ncAA#1)	687	707.8	704.1	4.23	0.65
Condition 1 Day- & Night-active (ncAA#1&2)	3256	3857.1	3811.6	5.98	0.74
Condition 2 Day- & Night-active (ncAA#1&2)	1891	2051.8	2060	4.70	0.62
Condition 2 Night-active (ncAA#2)	2352	2543.3	2479.5	5.56	0.72
Delaware Negative Control	22	22	22	1.32	0.43
DNA Extraction Negative Control	172	179	176.4	3.19	0.62

1169

1170

1171

1172

1173

1174